COMITATO NAZIONALE PER L'ENERGIA NUCLEARE
Laboratori Nazionali di Frascati

LNF - 67/73
4 Dicembre 1967

EXPERIMENTAL PROPOSAL FOR THE MEASUREMENTS OF THE PROCESSES: $e^+ + e^- \rightarrow \gamma + \gamma$; $e^+ + e^- \rightarrow \pi^o + \gamma$; $e^+ + e^- \rightarrow \eta + \gamma$.

R. Baldini-Celio, G. Capon, C. Mencuccini, G. P. Murtas, C. Pellegrini, A. Reale, M. Spinetti
Laboratori Nazionali di Frascati del CNEN

C. Bacci, G. Penso, G. Salvini
Istituto di Fisica dell'Università di Roma e Istituto Nazionale di Fisica Nucleare, Sezione di Roma

(Nota interna: n. 386)

Servizio Documentazione
dei Laboratori Nazionali di Frascati del CNEN
Casella Postale 70 - Frascati (Roma)

Laboratori Nazionali di Frascati del CNEN
Servizio Documentazione

LNF - 67/73

Nota interna: n. 386
4 Dicembre 1967

C. Bacci(x), R. Baldini-Celio, G. Capon, C. Mencuccini, G. P. Murtas, C. Pellegrini, G. Penso(x), A. Reale, G. Salvini(x) and M. Spinetti: EXPERIMENTAL PROPOSAL FOR THE MEASUREMENTS OF THE PROCESSES: $e^+ + e^- \rightarrow \gamma + \gamma$; $e^+ + e^- \rightarrow \pi^o + \gamma$; $e^+ + e^- \rightarrow \eta + \gamma$. (o)

This is a revised proposal on an experiment with the Adone storage ring, which is in advanced construction at the Frascati National Laboratories.

The intent of the experiment is the measurement of the cross section for the processes:

(1) $e^+ + e^- \rightarrow \gamma + \gamma$

(2) $e^+ + e^- \rightarrow \pi^o + \gamma \rightarrow 3\gamma$

(3) $e^+ + e^- \rightarrow \eta + \gamma \rightarrow 3\gamma$

and in general $e^+ + e^- \rightarrow n\gamma$ (apart from the obvious presence of radiative photons).

(x) - Istituto di Fisica dell'Università di Roma e Istituto Nazionale di Fisica Nucleare, Sezione di Roma.

(o) - This proposal is a revision and adjournament of our previous proposal on the same subject: LNF-66/4(Int); Proc. of the Int. Symp. on Electron and Positron Storage Rings, Saclay, sept. 1966, VII-3-5.

1. - REASONS FOR MEASURING PROCESSES (1), (2), (3). -

The interesting point in reaction (1) is the verification of electrodynamics (e. d.) for space-like values of the momentum of the virtual electron, in a momentum interval between 0. 1 and 2. 9 GeV.

This is of particular interest also in connection with recent measurements[1, 2] on the reaction γ + nucleus → nucleus + + $e^+ + e^-$.

In this reaction the propagator of the virtual electron for momenta between 0 and 0. 5 GeV is explored: R. B. Blumenthal et al.[1] found large deviations from the previsions of ordinary e. d. (including radiative corrections etc.). These deviations were incredibly large; to report the quantitative expression given from the authors, the ratio R of the experimental yield to the theoretical yield, is

$$R = 0.67 \left\{ (1 \pm 0.04) + (513 \pm 38)\, 10^{-8}\, M^2 \right\}$$

where M (in MeV) is the invariant mass of the $e^+ - e^-$ pair ($M^2 = -2Q_F^2$, Q_F = mass of the virtual electron). Of course this deviation, when confirmed, could also be due to some form factor correction in the photon-nucleus vertex: to get rid of this possible source of confusion (by working in a situation free from baryons) is one of the good reasons for using Adone.

A disconfirmation of the results of R. B. Blumenthal et al.[1] has already come from J. C. Asbury et al.[2]: these authors have found that R is very close to 1 ($R = 0.94 \pm 0.02 - (5.5 \pm 14.8) \times 10^{-8} M^2$), and there is no evidence of a deviation of quantum e. d. up to invariant masses of ~550 MeV. We incline to accept the result of Asbury et al.[2] as rather definitive up to this value. Our measurements of process (1) shall examine the same propagator, pushing the analysis to much higher momenta.

An interesting feature of process (1) is that it is more purely placed in the realm of e. d. than the processes

(4) $\qquad e^+ + e^- \rightarrow e^+ + e^-$

(5) $\qquad e^+ + e^- \rightarrow \mu^+ + \mu^-$

In fact in processes (4), (5), the virtual time-like photon propagator may be affected by deviations due to the vector mesons, like ρ, ω, φ.

Process (1) has an electron propagator, and therefore these deviations can influence it to a much lower extent (two e. m. orders less.

From an experimental point of view an important feature of reaction (1) is that it allows a check of q. e. d. by measuring the angular distribution at a given energy of e^+e^-. This is a great advantage, if one considers the difficulty of having in Adone, at least in a first stage, a monitoring system with a few percent accuracy.

The situation is different for the processes (2) and (3): in this case the propagator is concerning a time-like photon with a transferred momentum $k^2 = 4E^2$, 2E being the total c. m. energy.

A measurement of the cross sections (2) and (3) is obviously connected to the measurement of reaction (1) from the point of view of the experimental apparatus.

It is particularly convenient to look on the behaviour of these reactions in order to study the existence and behaviour of vector bosons. In fact the cross section of processes (2) and (3) can be relatively high when the total energy 2E approaches the mass of the vector bosons (ρ , ω, φ , . . .) then it strongly decreases to about 10^{-35} cm^2 when 2E is far from the mass of these resonances.

Measurement of processes (2) and (3) may constitute one of the best ways to measure $\omega - \varphi$ and $\eta - X^0$ mixing angles, and to check unitary theories in a rather new way; these arguments are developed in § 3.

Measurement of (2) and (3) is also a possible method to detect new vector bosons, rather independently from their coupling to the strong field.

2. - SOME DETAILS ON PROCESSES (1), (2), (3). PROCESS (1). -

a) In Born approximation reaction (1) is given by the following graphs:

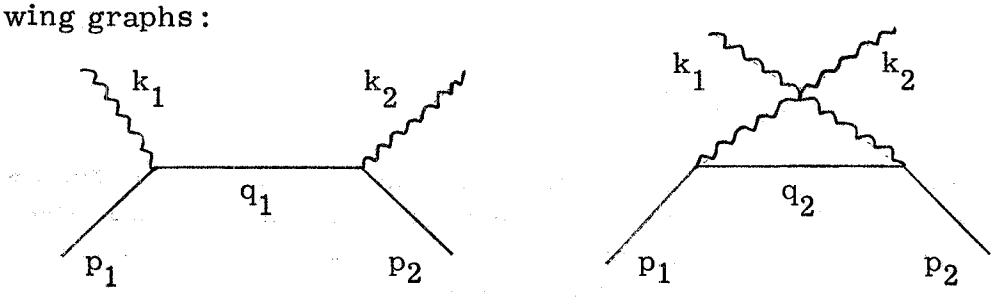

where

$$q_1^2 = 4E^2 \operatorname{sen}^2 \frac{\theta}{2}$$

(6)

$$q_2^2 = 4E^2 \cos^2 \frac{\theta}{2}$$

θ being the angle between the line of flight of the two photons and the e^+e^- direction (this angle is zero when the two photons are co linear with the electrons).

The cross section, valid for $\theta \gg 1/\gamma = m/E$, is[3]

$$(7) \quad \frac{d\sigma}{d\cos\theta} = \frac{\pi r_o^2}{\gamma^2} \frac{|F(q_1^2)|^2 \cos^4 \frac{\theta}{2} + |F(q_2^2)|^2 \operatorname{sen}^4 \frac{\theta}{2}}{\operatorname{sen}^2 \theta}$$

The form factor $F(q^2)$ is introduced to take care of possible deviations from q. e. d. , and can be thought as the product of the vertex and the propagator form factors :

$$F(q^2) = V_e^2(q^2) \cdot P_e(q^2) .$$

In Fig. 1 the cross section (7) is reported as a function of θ, for various energies of the electrons and assuming $Q=\infty$. To make an estimate of the possible deviations from the standard e. d. , we assume[3]

$$F(q^2) = (1 + q^2/Q^2)^{-1}$$

where we indicate by Q^2 the breakdown parameter. This is only an empirical parameter, whose theoretical inconsistency has been already discussed by N. M. Kroll[4].

Expression (7) may be rewritten in the form

$$Y = |F(q_1^2)|^2 + |F(q_2^2)|^2 \cdot X$$

with

$$Y = \frac{d\sigma}{d(\cos\theta)} \frac{\gamma^2}{\pi r_o^2} \frac{\operatorname{sen}^2 \theta}{\cos^4 \frac{\theta}{2}}$$

$$(8) \quad X = \operatorname{tg}\left(\frac{\theta^4}{2}\right) .$$

In Fig. 1a) the cross section values for this process are plotted as a function of E/Q. The strong dependence of the angular distribution on the value of E/Q indicates therefore that a first verification of e. d. may be already obtained by measuring, at two different angles θ_1, θ_2 the ratio $R = Y(\theta_1)/Y(\theta_2)$. This is shown in figures 2 and 3. In figure 2 the behaviour of Y for different values of E/Q as a function of $\operatorname{tg}^4(\theta/2)$ and θ is given. The lower graph is an enlargement at the smaller angles. In figure 3 we plot the ratio $R = Y(90^o)/Y(20^o)$ for various energies between 0. 3 and 1. 5 GeV.

As we see, R is close to 2 and energy independent, for $Q = \infty$, but it changes when $Q \neq \infty$. For instance, one can see that,

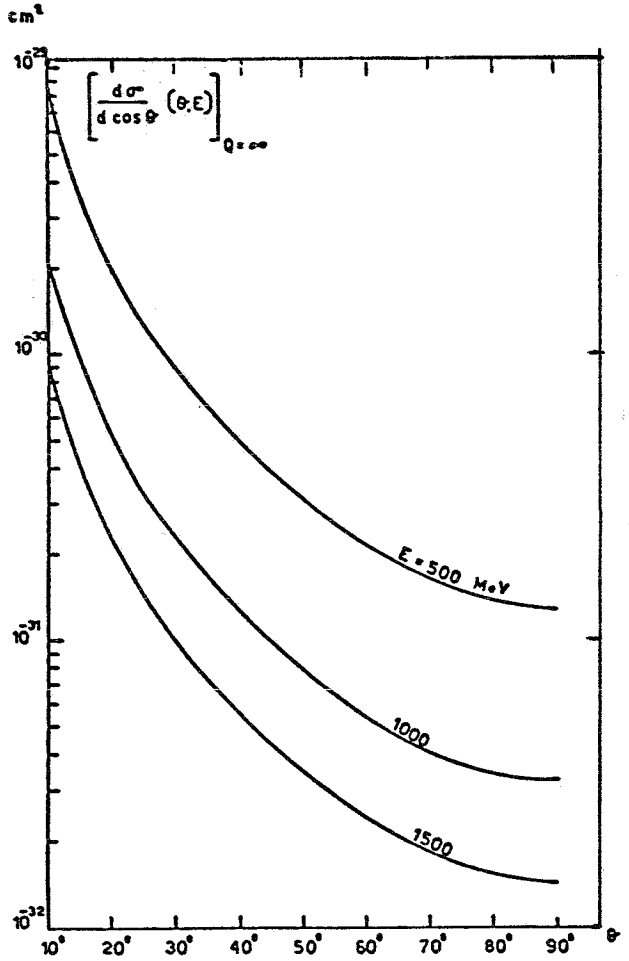

FIG. 1 - Differential cross section for reaction $e^+e^- \longrightarrow \gamma\gamma$ at 500-1000-1500 MeV according to standard Q. E. D.

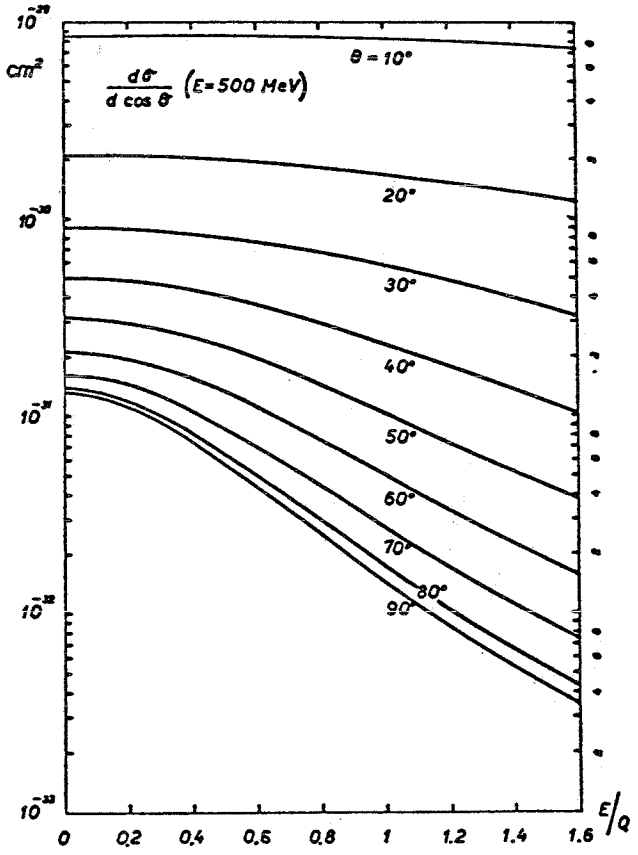

FIG. 1a - Differential cross section for reaction $e^+e^- \longrightarrow \gamma\gamma$ at 500 MeV for various values of the breakdown parameter Q.

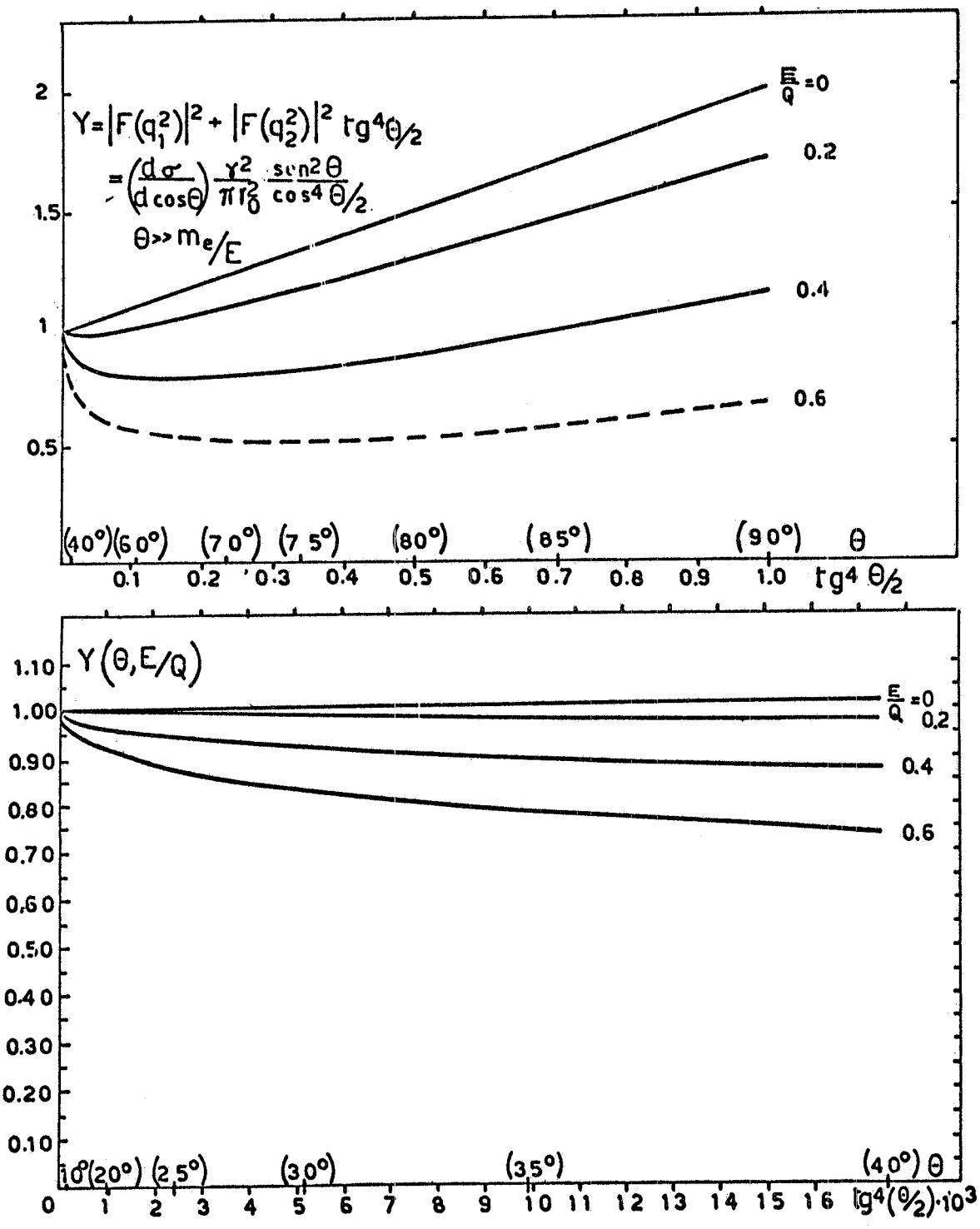

FIG. 2 - Plot of the quantity

$$Y(\theta, E/Q) = \frac{\gamma^2}{\pi r_0^2} \frac{\operatorname{sen}^2\theta}{\cos^4\theta/2} \frac{d\sigma}{d\cos\theta}$$

versus θ for various values of E/Q (E: energy of each electron beam).

at the maximum energy of Adone (E = 1. 5 GeV) and for Q = 5 GeV (corresponding to a length of the order of 4×10^{-2} Fermi^{-1}), the cross section deviates from the case Q = ∞ by ~ 28% at 90° and by ~ 2 % at 20°; correspondingly R = 1. 46.

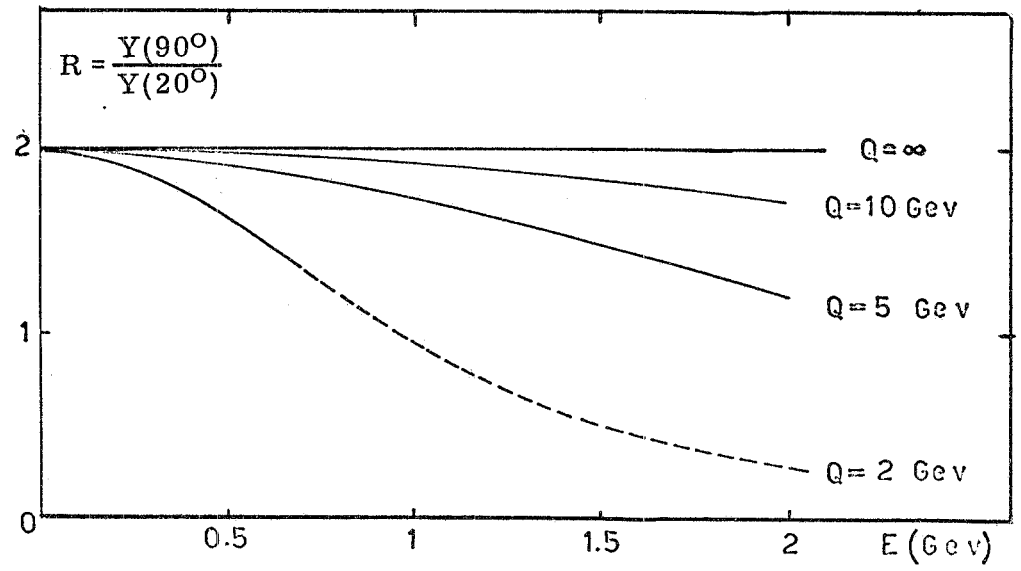

FIG. 3 - Plot of the ratio Y(90°)/Y(20°) versus the beam energy E for various values of the breakdown parameter Q.

b) Radiative corrections. In all the experiments with Adone, these are important corrections. Of course, the numerical evaluation of these corrections require the definition of the experimental apparatus, angles, momenta and errors on these quantities.

We limit ourselves here to an approximate evaluation, based on the recent calculations by Tsai[5].

This author has estimated the radiative corrections in case one single photon is revealed, emitted at an angle θ, with an energy indetermination Δw and angular indetermination $\Delta\theta$.

Let's assume that the experimental disposition reveals the two photons within a cone of total opening 2 $\Delta\theta$.

We can assume also[5] that the radiative losses are mainly in the form of a third photon, emitted in the direction of the e^+ e^- beams. In this case the minimum energy of one of the two annihilation photons revealed within the cone is E - Δw where

$$\Delta w = E \frac{\Delta\theta}{\Delta\theta + \text{sen}\,\theta}$$

and the corresponding maximum energy of the third photon is :

$$(9) \qquad k_3^{max} = 2E \frac{\Delta\theta}{\Delta\theta + \text{sen}\,\theta} \quad .$$

The expression given by Tsai[5] for the annihilation cross section in 2γ is

$$\frac{d\sigma}{d\Omega} = \frac{d\sigma_o}{d\Omega} (1 + \delta)$$

where

$$\delta = \frac{-2\alpha}{\pi} \left[(\ln \frac{E}{k_3^{max}} - \frac{3}{4}) (\ln 4\gamma^2 - 1) + \frac{f}{2} \right]$$

The cross section $d\sigma_o/d\Omega$ is given by (7); the function f is rather complicated, but it is relatively very small when

$$k_3^{max} << E \, .$$

By using the expression just given in (9) for k_3^{max}, we get the values given in Table I.

TABLE I

θ	$\Delta\theta$	E=500 MeV	E = 1000	E = 1500
20^o	2.5^o	$\delta = -0.056$	$\delta = -0.061$	$\delta = -0.064$
	5^o	$\delta = -0.019$	$\delta = -0.021$	$\delta = -0.022$
90^o	2.5^o	$\delta = -0.114$	$\delta = -0.125$	$\delta = -0.131$
	5^o	$\delta = -0.065$	$\delta = -0.071$	$\delta = -0.075$

The previous way to look to the problem is particularly valid when $\Delta\theta$ is fixed. This is not the case when using spark chambers as detectors.

Then one collects all the two γ's events whatever the angle between them and afterwards considers various values of $\Delta\theta$. For each $\Delta\theta$ value one has a certain δ and a certain background of events due to other processes.

One has then the possibility of chosing the $\Delta\theta$ value which gives a minimum value of δ and a maximum rejection against unwanted events.

On the other hand by varying $\Delta\theta$ it is possible to make a check on the evaluation of the radiative corrections.

3. - REACTIONS (2) AND (3), THAT IS $e^+ + e^- \to \pi^o + \gamma$; $e^+ + e^- \to \eta + \gamma$.

a) In Born approximation the processes (2) and (3) are described by the graph:

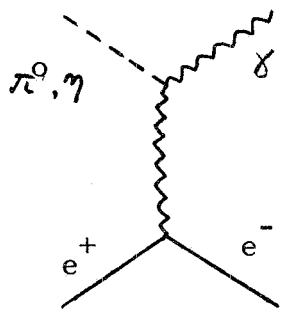

In the case of the π^o, the cross section is (page 127 of ref. (3)) :

$$\frac{d\sigma}{d\cos\theta} = \frac{\pi\alpha}{m_\pi^3}\frac{1}{\tau}\beta_\pi^3(1+\cos^2\theta) \times \left|\frac{G(4E^2)}{G(0)}\right|^2 \qquad (10)$$

where τ is the π^o life time, which is related to the pion form factor G from the relation

$$\frac{1}{\tau} = \frac{m_\pi^3}{64\pi}\left|G(0)\right|^2 . \qquad (11)$$

If we assume

$$\left|\frac{G(4E^2)}{G(0)}\right| = 1$$

the cross section (10) results to be $\sim 10^{-35}$ cm^2. An analogous expression will hold for the process $e^+ + e^- \to \eta + \gamma$, with the obvious substitutions of m_π, τ, β_π, and with a factor

$$\frac{\Gamma_{\gamma\gamma}}{\Gamma_{total}} = 0.4^{(6)} .$$

$\Gamma_{\gamma\gamma}$ being the width of the decay $\eta \to \gamma + \gamma$.

These are very small cross sections for Adone, but fortunately the interest of reactions (2) and (3) is connected to the more generous graphs, which we describe now in the following.

b) When the total energy of the system, 2E, is close to the mass of the vector bosons, an appreciable contribution may come from the graphs :

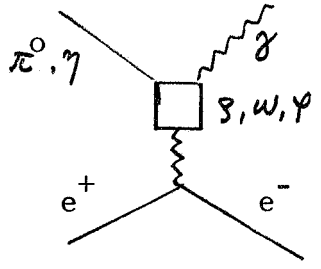

These graphs represent the electromagnetic production and decay of the known vector bosons ρ, ω, φ into the channels $\pi^o\gamma$ and $\eta\gamma$.

SU_3 theory makes previsions on the relative widths of these decays. Even more specific previsions can be drawn according to the quark model of the elementary particles. In this respect A-done seems to be a convenient machine to check these previsions experimentally.

As well known[3, 7], it is a good working hypothesis to assume that the nine known strongly interacting vector mesons ($\rho^{\pm o}$, K^{+}_{-}, K^{o}, $\bar{K}^{o}$, ω, φ) occupy a unitary octet and a unitary singlet. The mass difference between the elements of the octet fits the mass formula when one assumes a mixing of the singlet with the T=Y=0 member of the octet. For instance because of this mixing[8] the particle eigenstates, ω and φ, are linear combinations of ω_1 (the unitary singlet) and ω_8 (the T=Y=0 member of the octet) :

$$\begin{aligned} \omega_1 &= \omega \cos\theta_v - \varphi \sin\theta_v \\ \omega_8 &= \varphi \cos\theta_v + \omega \sin\theta_v \ . \end{aligned} \tag{12}$$

A similar mixing angle θ_p binds the η and X^o(mass 958) pseudoscalar mesons. In this situation there is a great interest in the measurement of the various electromagnetic decay modes ($\rho \to \pi^o + \gamma$; $\rho \to \eta + \gamma$ etc) of the ρ, ω, φ ; for instance the $\omega\varphi$ mixing angle θ_v can be measured in an independent way.

These electromagnetic decays depend on the coupling of the photon to the vector mesons: $G_{\rho\gamma}$, $G_{\omega_1\gamma}$, $G_{\omega_8\gamma}$. In the eightfold way limit, we have $G_{\rho\gamma} = \sqrt{3}\, G_{\omega_8\gamma}$, and $G_{\omega_1\gamma} = 0$, and for the matrix elements of the electromagnetic decay modes we obtain:

(13a) $\quad M(\omega \to \pi^o \gamma) \sim \sqrt{3}(g\cos\theta_v + f \operatorname{sen}\theta_v)$

(13b) $\quad M(\varphi \to \pi^o \gamma) \sim \sqrt{3}(-g \operatorname{sen}\theta_v + f\cos\theta_v)$

(13c) $\quad M(\rho \to \pi^o \gamma) \sim f$

(13d) $\quad M(\omega \to \eta\gamma) \sim g\cos\theta_v - f \operatorname{sen}\theta_v$

(13e) $\quad M(\varphi \to \eta\gamma) \sim -(g \operatorname{sen}\theta_v + f\cos\theta_v)$

(13f) $\quad M(\rho \to \eta\gamma) \sim \sqrt{3}\, f$

where f is[7] a coupling constant for the singlet vector and octet vectors interaction and g is a coupling constant for a D type interaction among the octet members.

The comparison of these previsions with the experiments may allow the determination of the f, g, θ_v constants, in a new ex

perimental way, and may constitute a rather independent check of the theory of mixing, as we already pointed out.

We observe since now that the decay mode $\varphi \to \pi^0 + \gamma$ could be really almost suppressed because experimentally[7,9] $G_{\rho\varphi\pi} \sim 0$. On the basis of his theory Glashow[7] anticipated that $\Gamma(\omega \to \pi^0\gamma) \cong \Gamma(\varphi \to \eta\gamma)$: this point should be verified by A- done rather easily. The quantity $\Gamma(\omega \to \pi^0\gamma)$, or at least the branching ratio $\Gamma(\omega \to \pi^0\gamma)/\Gamma(\omega \to 3\pi)$, has been measured by a number of authors[3,10]; the quantity $\Gamma(\varphi \to \eta\gamma)$ is much more in the air, as well as $\Gamma(\rho \to \eta\gamma)$.

Lindsey and Smith[11] give a limit for the value of the branching ratio relative to $\varphi \to \eta + \gamma$:

$$R_\varphi = \frac{\Gamma(\varphi \to \eta\gamma)}{\Gamma(\varphi \to \text{all modes})} = 0 \pm 8\% . \tag{14}$$

Badier et al.[12] give a limit $R_\varphi = 9 \pm 11\%$.

We can consider these results not in disagreement from what is deduced[11] from the calculations of Glashow[7,9]: $R_\varphi \approx 8\%$. In the following of the present proposal of the experiment we assume $R_\varphi \approx 8\%$. This value of R_φ has been confirmed in the recent calculations of Dalitz[13].

c) All this situation on the Vector $\to$ Pseudoscalar $+ \gamma$ decays may be pushed forward and becomes even more precise if we stick closely to the quark model for the elementary particles.

We shall present now the matrix elements (13) given before, in case we accept the quark model. In doing this we follow the lectures of R. H. Dalitz[13] at Les Houches, when treating the quark model for the pseudoscalar and vector mesons. In this case the constants f, g, of relations (13), are no more independent, and a theoretical prevision may be made for the mixing angles θ_V, θ_P. We sketch here very briefly the situation as developed in the quoted lectures of Dalitz.

The radiative transition $V \to P + \gamma$ can be classified according to the octet or singlet nature of V and P (where V and P indicates vector or pseudoscalar mesons) :

$$\begin{array}{ll} \text{A)}\ V_8 \to P_8 + \gamma & \text{C)}\ V_8 \to P_1 + \gamma \\ \text{B)}\ V_1 \to P_8 + \gamma & \text{D)}\ V_1 \to P_1 + \gamma \end{array} \tag{15}$$

These all are transitions of a magnetic dypole type M1 and their amplitudes, which we also indicate by A, B, C, D respectively, result proportional to the proton magnetic moment (the proton magne

tic moment does not appear here unexpected, for it is related to the quark magnetic moment). Remembering that[13] the photon transforms like the component of an octet (i. e. the Q = 0, U = 0 component), we can write a simple expression for the interactions (15), which allows us to establish definite relations between the amplitudes A, B, C, D. The relations are :

$$A = \mu_p/3 \; ; \quad B = C = \sqrt{6}\, A \; ; \quad D = 0 \tag{16}$$

In conclusion, following the quark model we arrive to very specific values and relations between the different decay modes, or radiative transitions, for the vector and pseudoscalar mesons. The values are given in the following two tables, II and III. Table II gi-

TABLE II

The amplitudes for the transitions $V \rightarrow P + \gamma$ according to SU_3 symmetry and quark model.

Process	Amplitude	Process	Amplitude	Process	Amplitude
$\rho^+ \rightarrow \pi^+ + \gamma$	A	$K^{*+} \rightarrow K^+ + \gamma$	A	$\omega_1 \rightarrow \pi^o + \gamma$	B
$\rho^o \rightarrow \pi^o \gamma$	A	$K^{*o} \rightarrow K^o + \gamma$	-2A	$\omega_1 \rightarrow \eta_8 + \gamma$	$B/\sqrt{3}$
$\rho^- \rightarrow \pi^- \gamma$	A	$\varphi_8 \rightarrow \pi^o + \gamma$	3A	$X^o \rightarrow \rho_o + \gamma$	C
$\rho^o \rightarrow \eta_8 + \gamma$	3A	$\varphi_8 \rightarrow \eta_8 + \gamma$	-A	$\varphi_8 \rightarrow X^o + \gamma$	$C/\sqrt{3}$

TABLE III

The predicted partial widths for the radiative meson decay processes listed, according to the quark model (Dalitz[13]).

Decay mode	M1 Amplitude (unit μ_p)	Predicted width
$\rho \rightarrow \pi\gamma$	$1/3$	120 keV
$\rho^o \rightarrow \eta\gamma$	$\sqrt{1/3}\cos\theta_p - \sqrt{2/3}\,\mathrm{sen}\theta_p$	70 keV
$K^* \rightarrow K^+\gamma$	$1/3$	70 keV
$K^{*o} \rightarrow K^o\gamma$	$2/3$	270 keV
$\omega \rightarrow \pi^o\gamma$	$\sqrt{2/3}\cos\theta_v + \sqrt{1/3}\,\mathrm{sen}\,\theta_v$	1.18 MeV
$\omega \rightarrow \eta\gamma$	$\sqrt{2}/3\cos(\theta_v+\theta_p) - 1/3\cos\theta_p \mathrm{sen}\,\theta_v$	7 keV
$\varphi \rightarrow \pi^o\gamma$	$\sqrt{1/3}\cos\theta_v - \sqrt{2/3}\,\mathrm{sen}\,\theta_v$	15 keV
$\varphi \rightarrow \eta\gamma$	$-1/3\cos\theta_v\cos\theta_p - \sqrt{2}/3\,\mathrm{sen}(\theta_v+\theta_p)$	240 keV
$\varphi \rightarrow X^o\gamma$	$-1/3\cos\theta_v\,\mathrm{sen}\,\theta_p + \sqrt{2}/3\cos(\theta_v+\theta_p)$	1 keV

ves the amplitudes for the mathematical elements of the octets and singlets. Table III, which is of direct experimental interest for us (p. 298, Dalitz) predicts the amplitudes and partial widths for each radiative meson decay of the physical particles, which may be a mixing of octets and singlets, according to the quark model. This table considers two mixing angles: one is the $\omega\varphi$ mixing angle, already reported before in (13) according to the work of Glashow; the other is the $\eta\eta'$ (or η-X) mixing angle θ_p. The amplitudes of table II agree with the matrix elements (13a-f) if we put

$$f = 1/3 \; ; \qquad g = \sqrt{2}/3 \; ; \qquad \theta_p = 0 \, .$$

To obtain from the amplitudes M of table II the partial widths, one must apply a space phase factor, which goes with the third power of the photon moment k in the reactions $V \rightarrow P + \gamma$:

$$\Gamma (V \rightarrow P + \gamma) \cong k^3 \, M_1^2 \, .$$

Every thing being fixed in this quark model, one can calculate, as Dalitz reported (p. 298), the absolute widths for each of the radiative decays.

These values are predicted in the last column of Table III.

d) Adone is therefore a rather unique instrument to check symmetric theories and mixing models through the $V \rightarrow P + \gamma$ decays. One particular aspect of the problem is worth mentioning[14].

The $\varphi \rightarrow \pi^o + \gamma$ amplitude has the form (see Table III)

$$M_{\varphi\pi^o} = \left(\frac{\sqrt{2}}{\sqrt{3}} \, \text{sen}\,\theta_v - \frac{\sqrt{3}}{3} \cos\theta_v \right) \mu_p$$

This amplitude vanishes in the case of special interest in which the $\bar{q}$ - q quark potential U does not depend on the quark label. This property holds automatically for the important case in which the potential results from the exchange of a vector coupled with baryons current. With this property, the potentials $\mathcal{U}\{8\}$ and $\mathcal{U}\{1\}$ are identical, therefore $m_8 = m_1$ for the vector meson states.

In this case the mixing angle θ_V is determined, being $\cos\theta_V = \sqrt{2/3}$; $\text{sen}\,\theta_V = \sqrt{3}/3$; $\theta_V = 35^o$, and $M_{\varphi\pi o}$ becomes zero[13]. The $\varphi \rightarrow \pi^o + \gamma$ mode is therefore, in this situation, forbidden. The study of the actual amplitude $M_{\varphi\pi o}$ is of interest to check the strength of this prediction. We know that it cannot be exact: in fact if we assume the actual mixing angle as descending from the real values of the masses m_ω and m_φ, we have $\theta_V \cong$

$\cong 40^{\circ}$ (p. 274). This value of θ_V makes $M_{\varphi\pi^0} \neq 0$, and precisely $M_{\varphi\pi^0} = -0.08\,\mu_p$.

This corresponds (see Table III) to a branching ratio $\Gamma(\varphi \to \pi^0\gamma)/\Gamma_{\text{total}} \sim 15/3000\ \text{kev} \sim 5 \times 10^{-3}$; this interesting number can probably still be measured in Adone.

The other process $\varphi \to \eta + \gamma$ is more abundant: $M_{\varphi\eta} = -0.48\,\mu_p$ and $\Gamma(\varphi \to \eta\gamma)/\Gamma_{\text{total}} \cong 8\%$. It can well be observed in our apparatus. The value of θ_p is not critical, and we may assume $\theta_p \cong -11^{\circ}$ (Dalitz, p. 278).

So, if we succeed to give evidence in Adone to the processes $\varphi \to \pi^0 + \gamma$; $\varphi \to \eta + \gamma$ we would have a new independent way to check the value of θ_V and the existence of the $\omega\varphi$ mixing at all.

In conclusion, the complete knowledge of the amplitudes for all the processes(15) $V_i \to P_j + \gamma$ (as given in Table III) could be of fundamental importance to verify SU_3. The point is now to try to foresee how well the processes (15) can be observed in Adone.

e) On the basis of what we said in § 3 a) b) c) d), we propose the measurement of the processes :

(17) $e^+ + e^- \to \varrho \to \pi^0 + \gamma$

(18) $e^+ + e^- \to \varrho \to \eta + \gamma$

(19) $e^+ + e^- \to \omega \to \pi^0 + \gamma$

(20) $e^+ + e^- \to \omega \to \eta + \gamma$

(21) $e^+ + e^- \to \varphi \to \pi^0 + \gamma$

(22) $e^+ + e^- \to \varphi \to \eta + \gamma$

at the energies 2E of $e^+ + e^-$ corresponding to the mass of the ϱ, the ω and the φ. The measurements of processes (2) and (3) will be extended also to other energy regions, considering that other bosons could exist, which did not appear yet in the usual strong channels.

We report in Fig. 4 the total cross sections for the processes (2) and (3). These cross sections have been calculated in the following way :

(i) We take the total cross section σ_{tot} for processes

$e^+ + e^- \to \varrho$; $e^+ + e^- \to \omega$; $e^+ + e^- \to \varphi$

from the calculation of R. Gatto[3].

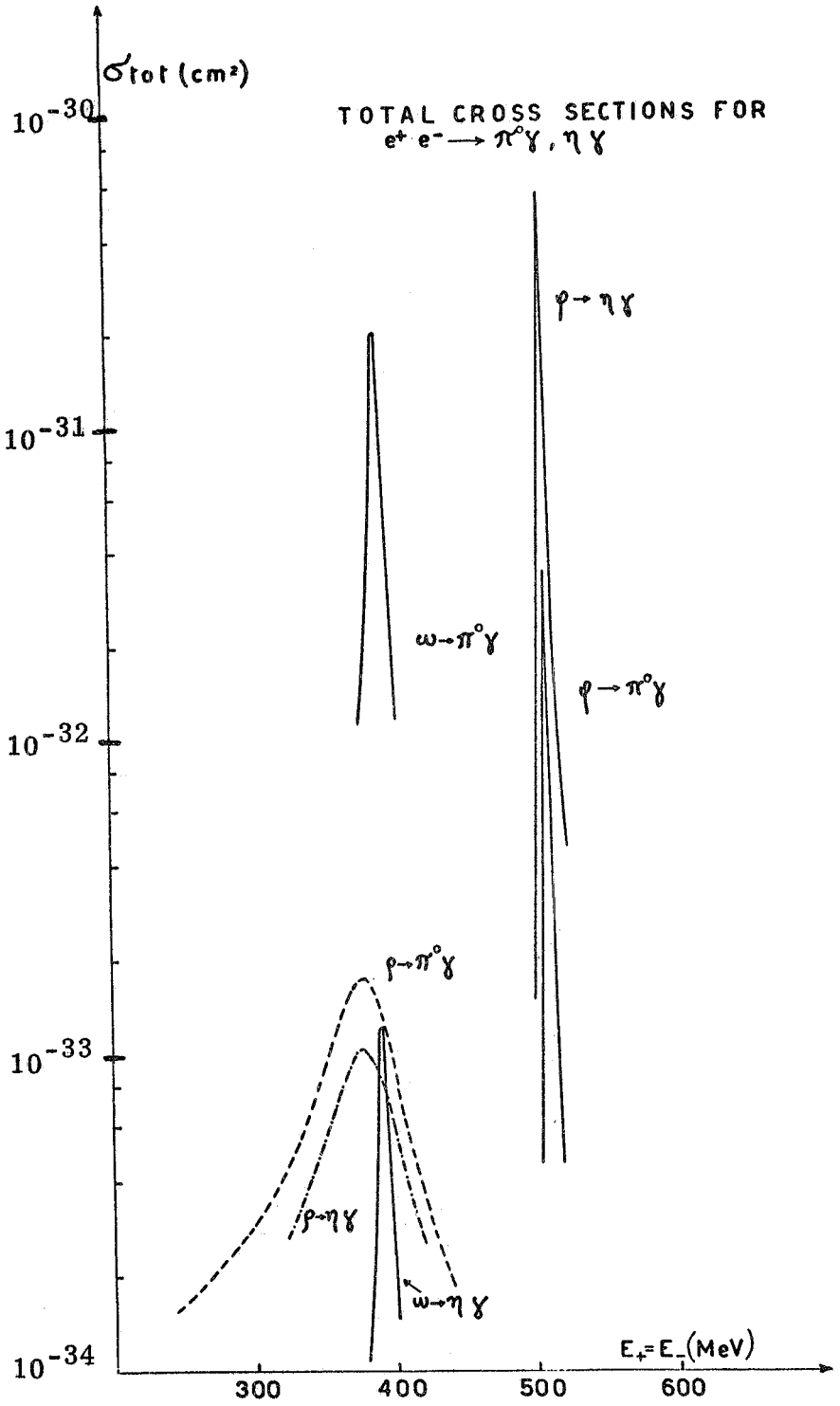

FIG. 4 - Total cross sections for reactions :

$$e^+e^- \rightarrow \pi^0\gamma \; ; \quad e^+e^- \rightarrow \eta\gamma$$

at the energies corresponding to the formation of the ρ, ω, φ resonances. For assumption made in the calculations see § 3 of the text.

(ii) We assume the following total widths :

Γ_ρ = 110 MeV ; Γ_ω = 9.5 MeV; Γ_φ = 3.1 MeV.

(iii) We calculate each cross section as given in Fig. 4 (for instance $e^+ + e^- \to \omega \to \pi^o + \gamma$), by multiplying the total cross section (for instance $e^+ + e^- \to \omega$, all modes) by the branching ratio relative to that mode, assuming the partial widths of Table III (for instance $e^+ + e^- \to \omega \to \pi^o + \gamma$ has the following cross section:

$$\sigma(\omega \to \pi^o \gamma) = \sigma_{tot} \frac{\Gamma(\omega \to \pi^o \gamma)}{\Gamma_{total}} = \sigma_{tot} \frac{1.18}{9.5}$$

It is important to remark that the cross sections for the processes $\rho \to \pi^o \gamma, \eta\gamma$ and $\omega \to \pi^o \gamma, \eta\gamma$ have been calculated neglecting the interference effects, which certainly are present.

The yield expected with the cross sections of Fig. 4 is estimates in § 11.

f) Radiative corrections. Also in reaction (2) and (3), of course, radiative corrections are important. The radiative corrections for these processes have not been evaluated until now. Anyway it is possible to make some qualitative considerations.

The first point is that, contrary to what happens for the two γ's annihilation, the measurement of $\pi^o + \gamma$ and $\eta + \gamma$ is done in poor geometry. This means that the value of K_3^{max} is defined by a $\Delta\theta$ equal to the overall half-aperture of the apparatus. Hence K_3^{max} could even be of the order of E itself and the radiative corrections, evaluated using the approximate formula

$$\delta = -\frac{4\alpha}{\pi} \ln \frac{E}{K_3^{max}} \ln 2\gamma \tag{23}$$

are rather small, of the order of a few percent.

On the other hand when the process goes through a narrow resonance, like the ω or φ, the shape of the cross section is substantially changed.

In fact if f(E,K)dk is the photon energy spectrum and $\sigma_o(E)$ the cross section for the process in absence of radiative corrections the observed cross section is

$$\sigma(E) = \int_{K_{min}}^{K_{max}} dK\, f(E,K)\, \sigma_o(E-K) \; . \tag{24}$$

Clearly this effect is bigger when the width of the resonance is smaller, and the resulting effect is a change of the shape of the

cross section versus E without a relevant change of the area defined by $\sigma(E)$.

g) From the point of view of the experimental abundance and possibility of observation of reactions (2) and (3), we can foresee the following :

ρ decays (17) (18). - The two processes have similar cross sections within a factor 2 (see Table III, or (13)) and the cross section is rather low. Both processes (2) and (3) will be difficult to observe, as appears in Fig. 4.

ω decays (19) (20). - Process $\omega \to \pi^o + \gamma$ is abundant, with a peak cross section of the order of 10^{-31} cm^2. Process $\omega \to \eta + \gamma$ should be very rare, at the limit of observation ($\sigma_{tot}(\omega \to \eta\gamma) \sim$ $\sim 10^{-33}$ cm^2).

φ decays. - The situation is reversed respect to the ω. The process $\varphi \to \eta + \gamma$ is abundant, and not difficult to observe. The peak value is $\sigma_{tot}(\varphi \to \eta\gamma) = 5.6 \times 10^{-31}$ cm^2. The "forbidden" process $\varphi \to \pi^o + \gamma$ is at the limit of detection, and its measurement is very interesting, as we said. The peak value is $\sigma_{tot}(\varphi \to \pi^o\gamma) = 3.5 \times 10^{-32}$ cm^2. In § 9 we shall give the expected yields per hour.

Two last points : Shui Yin Lo[15] has discussed the $e^+ + e^- \to$ $\to P+P$, $P+V$, $V+V$, $P+\gamma$ (P = pseudoscalar meson, V = vector meson) in the context of a meson pole model; M(12) symmetry with kinetic corrections (i. e. $SU(6)_W$ symmetry) is used to determine all the coupling constants. The total cross sections for the processes $e^+ + e^- \to P + \gamma$ are given, and are rather different from the previsions of the quark model we used.

V. V. Barmin et al.[16] have studied the events of the type $\pi^- + p \to n + X^o$ ($X^o \to \pi^o\gamma$) and obtained an evidence for a meson of mass 1300 MeV which has a $\pi^o\gamma$ decay mode. The quantum numbers for this new possible resonance are still very uncertain, and the case $J^P = 1^-$ could be possible. An analysis at a total energy of 1300 MeV in Adone with our apparatus is probably the best way to verify this hypothesis.

4. - CRITERIA FOR THE EXPERIMENTAL DETECTION. -

From what we said it appears the convenience of measuring at the same time reactions (1), (2) and (3): reaction (1) measures the possible anomalies of pure electrodynamics, and at the same time it is an "electrodynamic monitor" to reactions (2) and (3).

Let us now discuss the criteria for the distinction, from the experimental point of view, among processes (1), (2), (3).

As it will be evident from the following, a good angular resolution will be necessary for an unambiguous distinction among the three reactions. This resolution has been estimated for our apparatus (see appendix A) and results to be $\leq 1.8^{\circ}$ when the direction of γ ray of 500 MeV is measured through the development of the shower in the spark chambers. Moreover if we know a priori or if we reconstruct the position of the interaction region for the colliding beams we can assume (for events coming from the interaction region) a resolution in the φ angle when looking in the xy plane of the order of 0.3°. This comes from the fact that the transversal cross section of the electron beams will have dimensions $\Delta x \Delta y = 5 \times 0.1\ mm^2$ and the origin of the shower in the spark chambers may be determined within ± 1 mm.

The $e^+e^- \rightarrow \gamma\gamma$ events will give two photons very well aligned in the φ view (xy plane) (within the experimental resolution) because the radiative photons are emitted with very good approximation along the beam direction (z axis). In the θ view these photons will be aligned within an angle $\Delta\theta$ depending on the entity of the radiative losses (see Table I).

Processes (2) and (3) have three photons in the final state. The angular correlations between these photons are rather different for the $\eta\gamma$ and $\pi^{\circ}\gamma$ case. In fact the angular distribution of the decay photons depends only on the velocity β of the decaying particle and we have :

$$
\begin{array}{lll}
\beta_{\pi^0} = 0.942 & \beta_{\eta} = 0.337 & \text{at the } \omega \text{ resonance} \\
\beta_{\pi^0} = 0.966 & \beta_{\eta} = 0.551 & \text{at the } \varphi \text{ resonance .}
\end{array}
\tag{25}
$$

As an example, to fix ideas, we give in Fig. 5, the probability $P(\theta)$, for unit solid angle, of emitting a decay photon at angle θ respect to the π° or η direction. In figure are shown the curves for the π° and η case calculated at the φ resonance.

The efficiencies of our apparatus for detecting all three or only two γ's have been computed and are reported in § 9. Because the three γ's efficiency is rather low we think to use also events with only two photons detected. Let us discuss separately these two cases :

I) Events with 3 γ's detected.

We may exclude that these may be events from annihilation, one of three γ's being a radiative photon, because we detect only photons with θ, $\pi - \theta \geq 20^{\circ}$ so that is highly improbable to have a

radiative photon in our apparatus. Then we can assign each event to reaction (2) or (3) looking at the respective angles of the three photons. In fact, as we know the initial state, from the measurement of the directions, we are able to calculate the energies of the three photons and then to see if the invariant mass of a couple of them corresponds to the π^0 or η mass.

II) Events with 2 γ's detected.

In this case the kinematics is not determined; distinction among reactions (1), (2), (3) could be easily obtained if, beyond direction, we could measure also the photon energy; but, for the moment, this is accomplished by our apparatus only with poor resolution.

We have calculated with a Montecarlo method, for our experimental conditions, the distributions of two angles $\Delta\alpha$, $\Delta\varphi$ [$\Delta\alpha = \pi - \hat{\vec{K}_1 \vec{K}_2}$; $\Delta\varphi = (\vec{K}_1, \vec{Z})(\vec{K}_2, \vec{Z})$], defined for the two detected photons (these may be either the primary photon and a decay photon or both the decay photons). Preliminary results show that the distributions for the η and π^0 case are quite different, so that it should be possible, to fit the experimental distribution with their sum. Leaving as free parameters the yields from reactions (2) and (3), from a best fit one should then obtain the separation between the $\pi^0\gamma$ and $\eta\gamma$ events (see Figg. 5b and 5c).

The annihilation events in a $\Delta\alpha$, $\Delta\varphi$ plot will be grouped in a narrow peak, moreover their contribution should be easily measured when shifting the machine energy outside the resonance peak.

5. - OBSERVATION OF THE RADIATIVE PHOTON. -

From what we said it is clear that the radiative corrections in all processes (1), (2) and (3) are rather important, and the "third photon" may have rather high energies (for instance 10-100 MeV). Without a great accuracy in the calculations of the radiative corrections it would be difficult to discover with certainty any "breakdown" of electrodynamics, unless it had the catastrophic dimensions indicated in the experiment of Cambridge[1].

It may therefore be a good criterium, for the radiative corrections, to observe and measure the radiative photons, by placing a detector on the z axis (zero degree counter), and counting N(K)dK, that is the energy spectrum of the photons observed on the z axis and in coincidence with reactions (1), (2) or (3). This relevant information is added to the others, without being involved in the general triggers of the spark chambers and the hodoscopes.

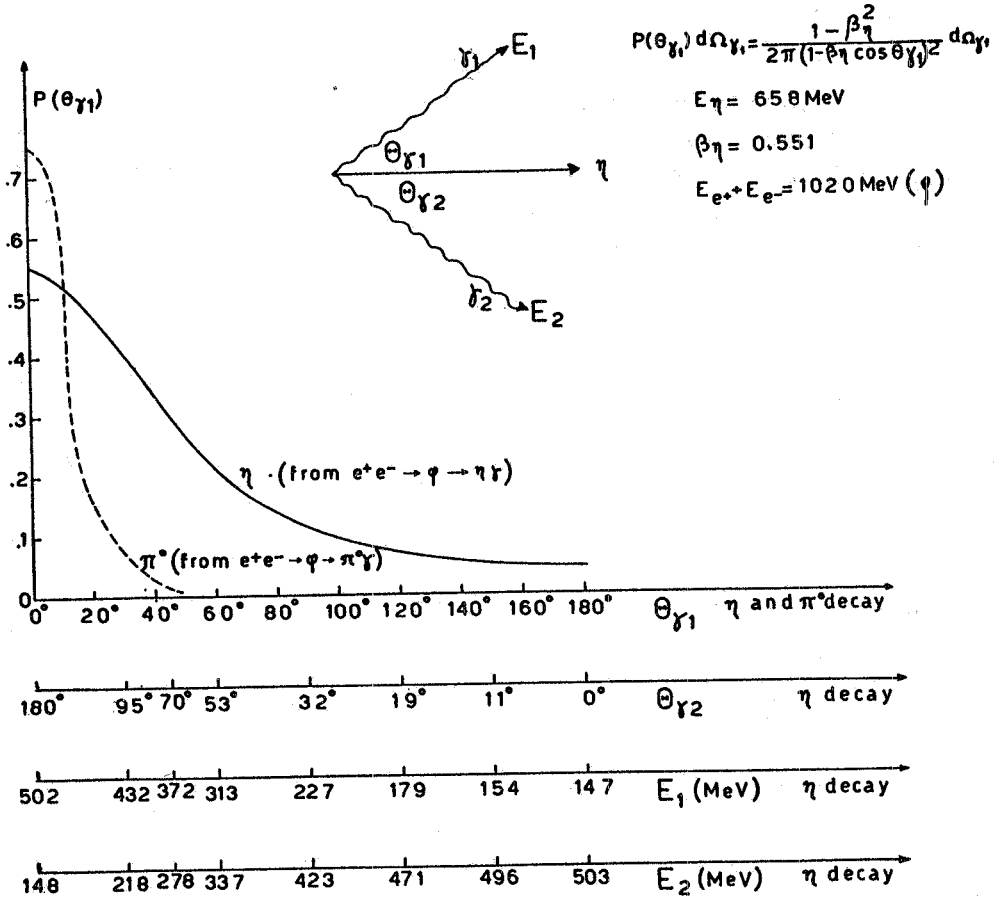

FIG. 5 - Plot of the probability $P(\theta\gamma_1)$, per unit solid angle, of observing a photon γ_1 from the η (or π^0) decay at angle $\theta\gamma_1$ respect to the η (or π^0) direction. The η (π^0) has an energy of 658 MeV (519 MeV) corresponding to the process $e^+e^- \to \varphi \to \eta\gamma(\pi^0\gamma)$. The lower abscissa scales are valid only for the η decay and give respectively :

the angle $\theta\gamma_2$ of the second decay photon;
the energy E_1 of the first decay photon;
the energy E_2 of the second decay photon.

FIG. 5b - This figure refer to those events $e^+e^- \to \pi^0\gamma, \eta\gamma$ at the φ resonance, in which only two γ's are detected and the third one does not cross our apparatus. The angular deviations $\Delta\alpha$, $\Delta\varphi$ are defined as :

$\Delta\alpha = \pi - \vec{K}_1 \hat{\vec{K}}_2$ $\quad$ $\vec{K}_1, \vec{K}_2$: photons momenta

$\Delta\varphi = (\vec{K}_1, \vec{Z}) \cdot (\vec{K}_2, \vec{Z})$ $\quad$ $\vec{Z}$: beam direction.

In figure is shown the distribution of the $\pi^0\gamma$ and $\eta\gamma$ events expected for our apparatus, computed by a Montecarlo method.

→

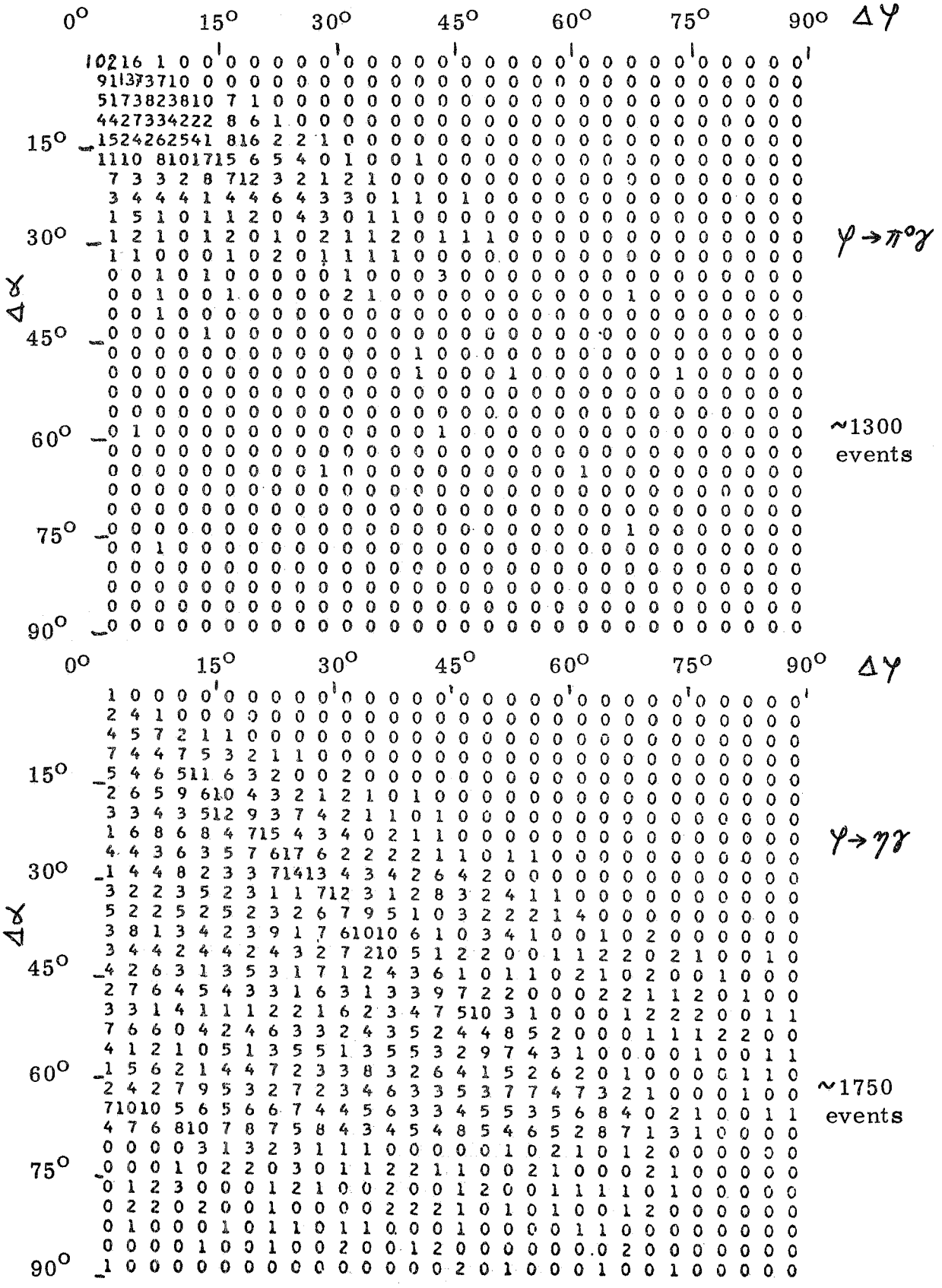
0° 15° 30° 45° 60° 75° 90° Δγ
Δα
15° 30° 45° 60° 75° 90°
γ→π°γ
~1300 events
γ→ηγ
~1750 events

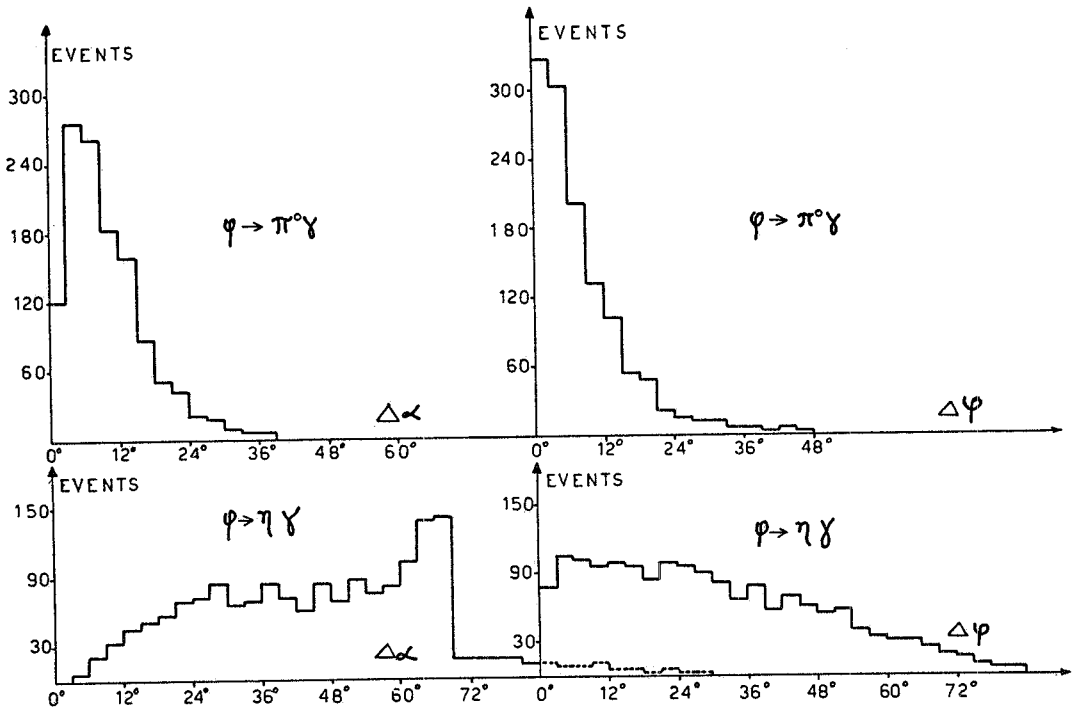

FIG. 5c - Distribution of the events versus $\Delta\alpha$ ($\Delta\varphi$) when integrating the distribution of fig. 5b over $\Delta\varphi$ ($\Delta\alpha$).

We consider this point important, if experimentally possible. The resolving power of the detectors allows us to hope that the "third photons" when the energy is beyond 10 MeV or so, may be separated from the background.

6. - SOME REMARKS ON THE EXPERIMENTAL PROCEDURE FOR PROCESS (1). -

As we previously said in § 2, verification of electrodynamics may be based, in reaction (1), on the angular distribution of the two photons respect to the e^+e^- axis. This may be made by measuring the ratio R between (§ 2) the Y function at angle θ and the Y at a fixed angle θ_o, the "monitoring angle". For instance, by assuming $\theta_o = 20^o$:

$$(26) \qquad R = \frac{Y(\theta)}{Y(20^o)} = \frac{C(\theta,E)}{C(20^o,E)} \frac{\mathcal{E}(20^o)}{\mathcal{E}(\theta)} f(\theta) ,$$

when

$$f(\theta) = \frac{\text{sen}^2\,\theta\,\cos^4(20^o/2)}{\text{sen}^2(20^o)\cos^4(\theta/2)} ;$$

$\mathcal{E}(\theta)$ = detection effi ciency ;

C = Trigger rate x $\frac{\text{good pictures}}{\text{total n. pictures}}$ = $\gamma\gamma$ experimental rate .

It is clear that in order to investigate the behaviour of R as a function of the energy we need $\mathcal{E}(20^o)/\mathcal{E}(\theta)$ being energy independent, or at least, we must control how it depends from the energy of the photons to be detected. We can check this using a calibrated beam of electrons or γ's and experimental work on this point has been carried out (see appendix A).

This is also the reason why we should have the spark chamber disposition quite symmetrical at different θ angles.

7. - THE EXPERIMENTAL APPARATUS. -

The experimental apparatus is given in Figg. 6, 7, 8 and 9. The general disposition is sketched in Fig. 6.

The trigger for the events interesting processes (1), (2) and (3) is made by large plastic scintillators, of increasing dimensions, from 40×30 cm^2 to 100×110 cm^2. The recognition of the events and their identification is made by taking pictures of a system of spark chambers. This system of spark chambers is an assembly of two gap independent units of different dimensions, from a size of $\sim 30 \times 40$ cm^2 to a maximum size of 100×100 cm^2.

The main advantage of this system is the exploration of a rather large angular region in θ (from a minimum of $\theta = 15^o$ to a maximum of $\theta = 135^o$) with the advantage of having rather equal impact angles for γ rays emitted at very different values of θ.

Two possible arrangements of the chambers and counters are shown in figg. 7 and 8. Essentially they differ only for a more or less uniform distribution of the materials (converters and absorbers) between the chambers.

The first two-gap chambers are used as anticoincidences, to be sure that we are dealing with gamma rays. Next comes the scintillator S_o in anticoincidence and then the absorbers, chambers and counters in a suitable array.

The trigger for the spark chambers is given by the coincidence (see Fig. 7) :

$$T = \bar{S}_o + \bar{S}'_o + S_i + S_j + S'_k + S'_l \qquad i,j,k,l = 1,2,3 \tag{27}$$

(Scintillators $S_o S_i S_j$ and $S'_o S'_k S'_l$ can be either horizontal or inclined ones. We plan to take all the coincidences of type (27) between any two of the four blocks of chambers).

We mean here that when $i = j$ or $k = l$, $S_i + S_j = S_i$ and $S'_k + S'_l = S'_k$. Note that in the case $i \neq j$ (or $k \neq l$) we have a double coinci-

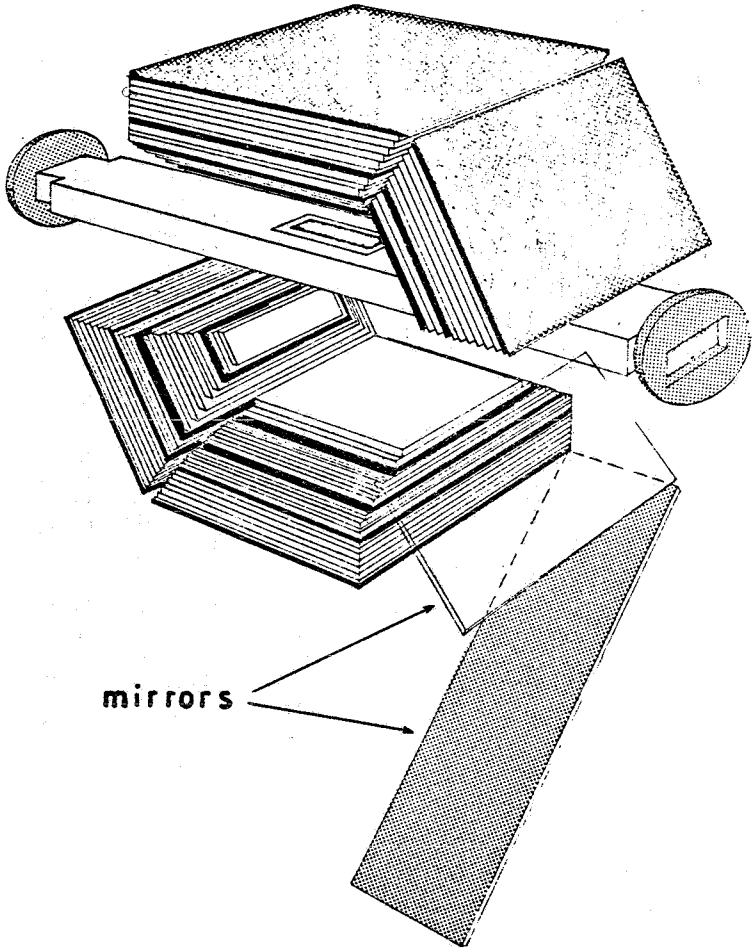

FIG. 6 - Perspective view of the experimental apparatus.

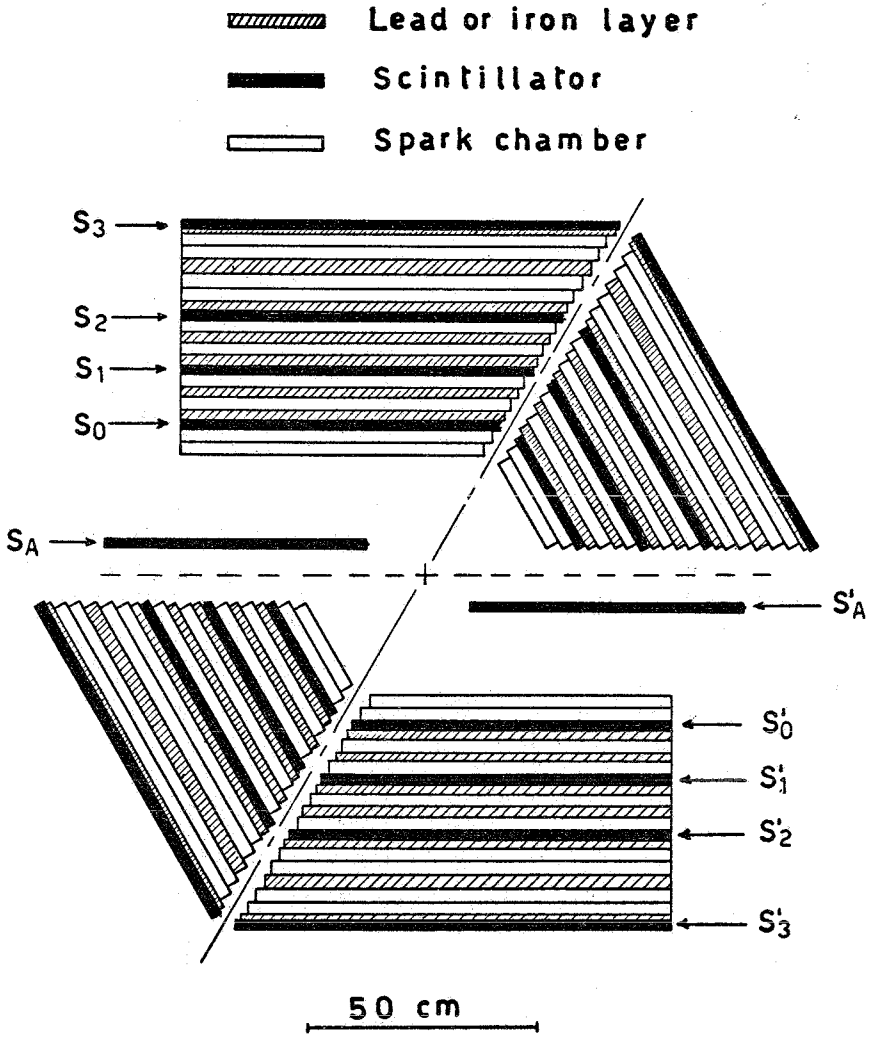

FIG. 7 - Vertical section of the experimental apparatus along the beams direction. Scintillators S_A, S'_A are intended to be used to anticoincide cosmic rays not passing through the interaction region.

dence to define a single γ so that the contribute of the background is reduced respect to the photons due to true events. Of course also the efficiency of detection of the "true" photons gets reduced (see appendix A and B) but to a smaller extent, especially in the case of the photons of high energy ($\geq$ 500 MeV).

A number of experimental tests have already been made (appendix A) and a Montecarlo program is being developed in order to have indication on the best efficiency of the trigger as a function of the absorbers and converters, and the best disposition of the spark chambers, to reach the maximum precision in the localization of the e. m. showers: it is important to underline that the knowledge of the axis and some possible knowledge of the energy of the shower, will be of great importance in all reactions (1), (2) and (3).

One experimental disposition foresees, immediately or in a second time, the addition of other spark chambers with heavy absorbers (iron plates). It will be possible to measure with them the angular distribution in θ of any charged particle pair, with the possibility of distinguishing the pions from the muons. The preliminary indication of the experimental disposition is given in Fig. 9. The mechanical structure shown in Fig. 9 is the same we are preparing for the disposition of Figg. 6, 7, 8.

The iron spark chambers will be photographed only in the front view.

Optics, camera and mirrors.

Pictures of the e. m. showers in the spark chambers will be taken from the front (viewed as in Figg. 7, 8) and from the side. The side view will take also the image of the tracks from the spark chambers inclined at 60° through an adeguate optical transfer (total reflexion prisms). This disposition is perhaps rather new, and is described in appendix D, together with the mirrors, which must resolve the problem of extracting the image from the narrow space of the Adone straight sections.

We decided for a 70 mm film, in view of the detailed information we must report on each photograph. We also decided to avoid spherical and cylindrical lenses between the spark chambers and the camera. In fact the pictures will be taken from very far (from "infinite", that is at least 25-40 m) with a teleobiective. This system has been already studied, and seems to work satisfactorily (see app. D).

Our system is constructed with the possibility of introducing major changes in the disposition: in this respect we decided for many two-gap spark chambers. The mechanical support (Fig. 9) is such that the higher half can slide respect to the lower part, with a

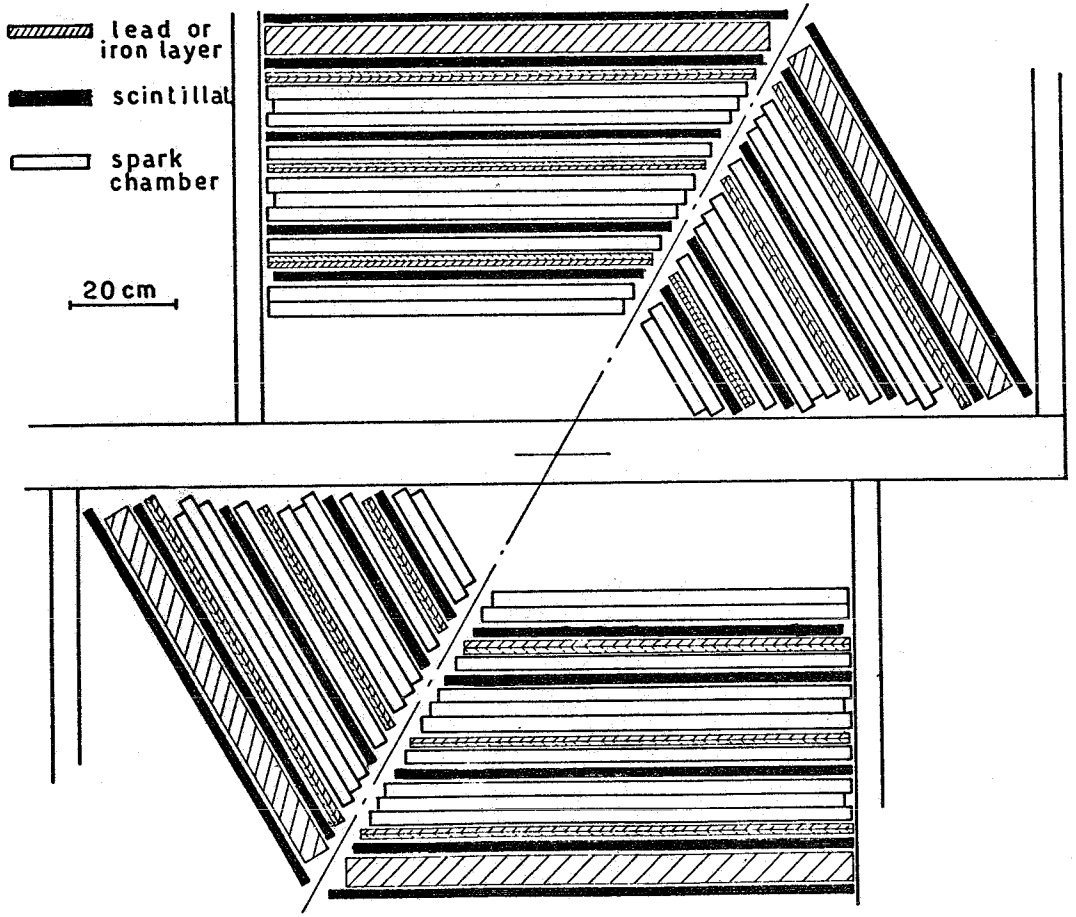

FIG. 8 - As in fig. 7 with an alternative disposition of the converters between the spark chambers. Here is also shown the lead shielding after the last spark chambers and the subsequent anticoincidence counter.

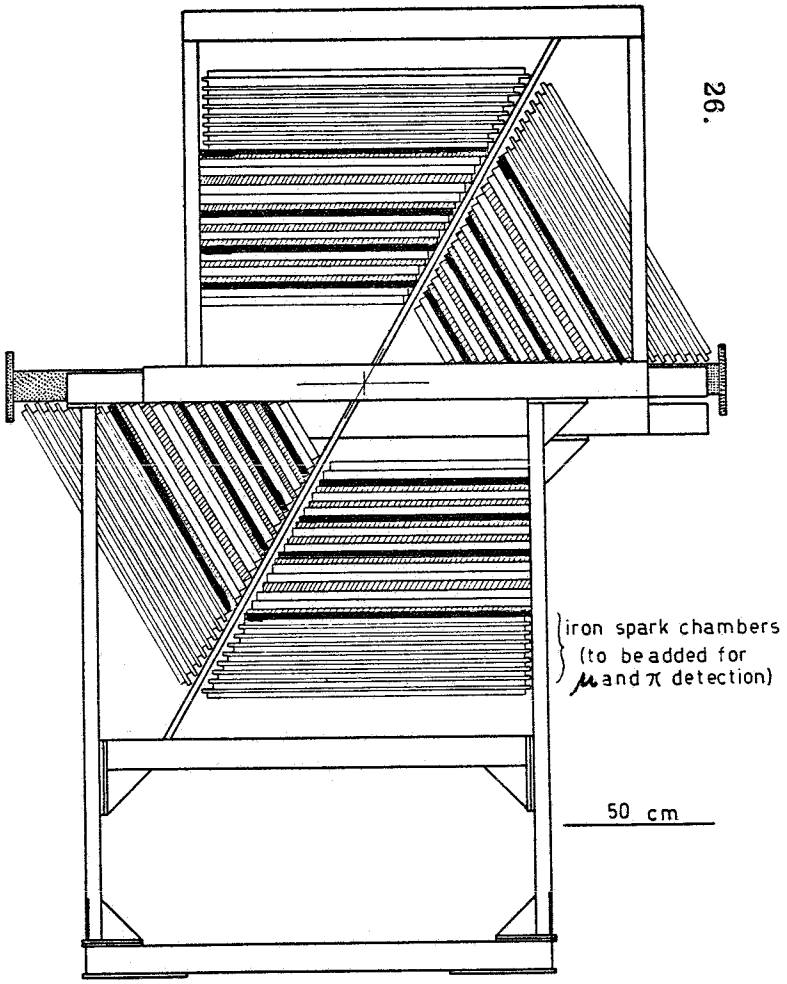

FIG. 9 - View of the apparatus together with its mechanical support. Here are also shown the iron spark chambers which shall be added to detect μ and π mesons.

significant change of the position of the spark chambers respect to the crossing region; this will be useful to avoid systematic errors due to differences in efficiency of the scintillators, spark chambers, etc.

The solid angle covered by chambers around the crossing area is close to 4 steradiants. This is rather good for process (1), and not bad for process (2). Process (3) is more difficult to detect, expecially for the fact that the three photons are emitted at rather angles (§ 9).

The scintillators are rather large ($\sim$ 1 squaremeter) and the photomultipliers for them should not disturb the observation of the s. c. We plan to put 2 (or 3) 56 AVP p. m. on one side only of each scintillator (on the back of Fig. 7). The tests we already did confirm this possibility.

8. - COSMIC RAYS. -

Because of the rather low counting rates, cosmic rays may be a dangerous background in all Adone experiments. We estimate that coincidences $S_i + S_j + S_k + S_l'$ (see § 7) due to cosmic rays (in case they are not rejected by the time resolution) are in our apparatus of the order of 2-3000 per minute. They shall be mostly μ mesons and e. m. showers. A good covering roof of 10 to 15 cm of lead over our apparatus can reduce almost entirely the cosmic ray background to the μ mesons.

When we are treating processes (1), (2), (3) the anticoincidences S_o, S_o' (see Fig. 7) shall reduce the cosmic ray background by a large factor. But when measuring charged particles from the crossing region, the situation becomes rather bad. We plan to reduce or eliminate the cosmic rays by use of the following criteria, which of course do not exclude each other :

- to exclude coincidences not in time with the e^+ and e^- bunches of the circulating beams;
- to use a time of flight method, so that the difference in time of flight between cosmic rays and particles emitted from the crossing region can be used to eliminate cosmic rays. This method looks rather promising and some results are reported in app. G;
- to set an anticoincidence over the lead roof;
- to place an horizontal anticoincidence S_A at both sides of the donut (see Fig. 7), so that only the cosmic rays going grossly through the crossing region may be admitted: should these coincidences not be overcrowed, this obvious procedure would bring a great advantage.

Other methods (directional counters, etc.) are being considered by our group as well as other groups around Adone.

9. - COUNTING RATES. -

We assume a machine luminosity L given by the formula:

$$L = 10^{33} \frac{E\ (GeV)}{1.5} \qquad (cm^2 \times hour)^{-1}$$

which is the project value for Adone.

a) $e^+e^- \rightarrow \gamma\gamma$.

The counting rates have been calculated integrating the differential cross section $d\sigma/d\cos\theta$ (assuming the validity of Q. E. D.) over the θ, γ acceptance of our experimental apparatus (see Figg. 6; 7, 8, 9). The results are summarized in Fig. 10 and in Table IV. We have assumed an overall efficiency detection equal to 80%. On the other side we believe that the geometrical acceptance of our apparatus may be still be improved.

The total counting rates for the $\theta = 30^o$ and the $\theta = 90^o$ chambers are respectively : 34 and 17 events/hour at E = 500 MeV; 11 and 5. 5 events/hour at E = 1500 MeV.

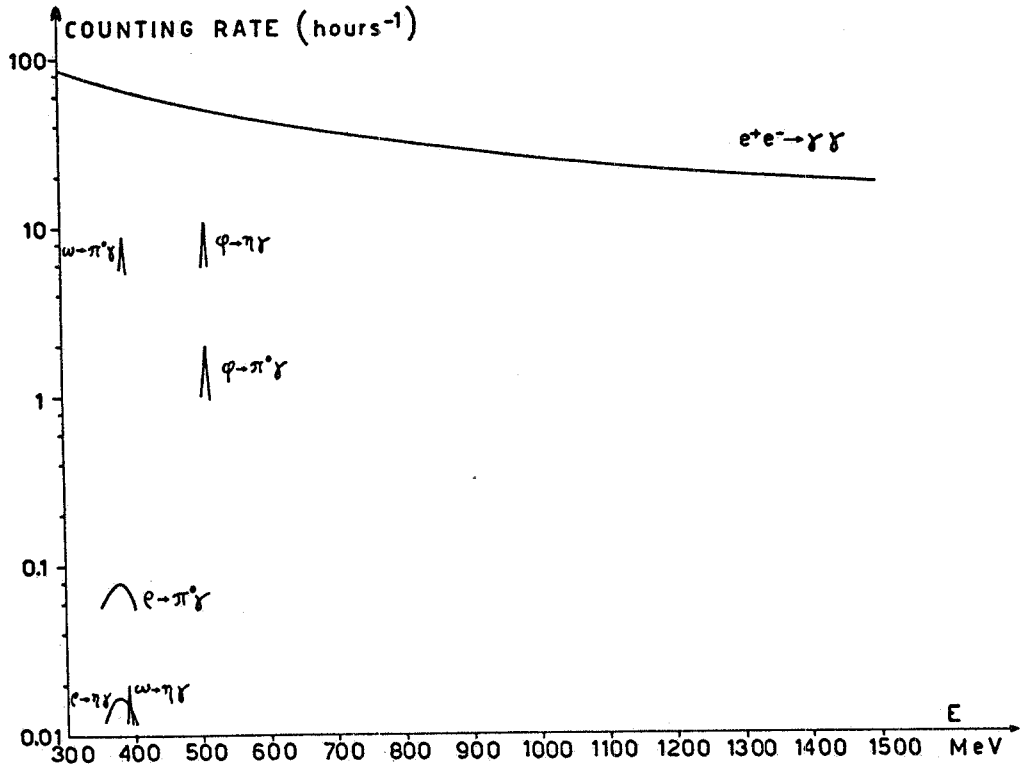

FIG. 10 - Total counting rates expected for reactions : $e^+e^- \rightarrow \gamma\gamma$; $e^+e^- \rightarrow \pi^o\gamma$; $e^+e^- \rightarrow \eta\gamma$.

TABLE IV

$e^+e^- \rightarrow \gamma\gamma$ counting rates

E	θ	$d\sigma/d\cos\theta \times 10^{32}$ (cm^2/sterad)	Events/hour
500	$(30 \pm 5)^\circ$	90	12
500	$(90 \pm 5)^\circ$	13	2.4
1500	$(30 \pm 5)^\circ$	10	4
1500	$(90 \pm 5)^\circ$	1.45	0.8

b) $e^+e^- \rightarrow \pi^\circ\gamma, \eta\gamma$.

In the following we assume to detect the reaction $e^+e^- \rightarrow \eta\gamma$ observing the decay $\eta \rightarrow \gamma\gamma$. We use for this decay the branching ratio ($\eta \rightarrow \gamma\gamma$ / $\eta \rightarrow$ all) = 0.4.

However we are studying also the possibility of observing also the decays $\eta \rightarrow \pi^+\pi^-\pi^\circ(\gamma)$, $\eta \rightarrow 3\pi^\circ$, $\eta \rightarrow \pi^\circ\gamma\gamma$. As

TABLE V

Reaction	Luminosity ($cm^{-2}\ h^{-1}$)	Events produced per hour	2γ geometrical efficiency	3γ geometrical efficiency	2γ rate (h^{-1})	3γ rate (h^{-1})
$\omega \rightarrow \pi\gamma$	0.26×10^{33}	52	0.20 (0.22)	0.08 (0.10)	6.7	2.1
$\omega \rightarrow \eta\gamma$	0.26×10^{33}	0.31	0.21 (0.24)	0.04 (0.06)	0.017	0.003
$\varphi \rightarrow \pi\gamma$	0.34×10^{33}	12	0.19 (0.19)	0.09 (0.14)	1.5	0.56
$\varphi \rightarrow \eta\gamma$	0.34×10^{33}	190	0.21 (0.25)	0.026 (0.04)	10	1.0
$\rho \rightarrow \pi\gamma$	0.26×10^{33}	0.47	0.20 (0.22)	0.08 (0.10)	0.06	0.02
$\rho \rightarrow \eta\gamma$	0.26×10^{33}	0.27	0.21 (0.24)	0.04 (0.06)	0.015	0.002

we said in § 4, we have for these reactions three γ's in the final state but we keep also events in which only two γ's are detected.

We have computed the geometrical efficiency for having 2γ or 3γ in our apparatus by means of a Montecarlo method. The corresponding results are reported in Table V. The geometrical efficiency in the 3γ case and to a smaller extent in the 2γ case, is strongly dependent on the solid angle acceptance. Therefore in Table V we report in parentheses also the efficiencies calculated with larger θ and φ acceptance than strictly predicted for our apparatus (11% more of solid angle) in case we succeed in reducing the dead angles.

In Table V are also shown the 2γ and 3γ counting rates. These contain also the γ detection efficiency: we assume the probability to see a single γ to be 0.8. The $\eta\gamma$ counting rates contain the $\eta \to \gamma\gamma$ branching ratio. The counting rates and efficiencies have been calculated at the energies corresponding to the formation of a ρ, ω, φ resonance. We have used the values of the cross sections reported in § 3. As we already said the ρ decays ($\eta + \gamma$ and $\pi^0 + \gamma$) and the ω decay into $\eta + \gamma$ shall be impossible to observe; the counting rates for $\omega \to \pi^0\gamma$ and for $\varphi \to \eta\gamma$ are still possible with the present luminosity.

10. - BACKGROUND. -

We mean by background the unwanted events, and in particular those uninteresting ones that do not come from beam-beam interactions. We hardly know, at present, the percentage of unwanted photos and of useless triggers we will have: it seems sure, considering the recent progresses with some other e^+e^- colliding beams (Saclay, ACO) that this background shall be a strong function of the general conditions of the machine (vacuum, dimensions of the beam) and the shieldings.

Let's examine anyway the background due to some of the processes which can simulate reactions (1), (2), (3).

a) Events recorded as $e^+ + e^- \longrightarrow \gamma\gamma$ in the chambers looking to small θ value (the non horizontal chambers), due to an accidental coincidence between two single bremsstrahlung γ's.

Of course, this effect can in case be important only at small angles. If one assumes in the region $10^o < \theta < 40^o$ at $E = 1.5$ GeV a total cross section of $\sim 5 \times 10^{-31}$ cm^2 for single bremsstrahlung[17], which corresponds to a threshold $\simeq 0.01\,E$ in the energy spectrum of the radiated photons, the number of accidentals comes out to be really negligible.

b) Events $e^+e^- \rightarrow e^+e^-$ recorded as $e^+ + e^- \rightarrow 2\gamma$ because of high energy bremsstrahlung of the outcoming electrons in the wall of the donut.

This possibility is important to us when only γ rays arrive to the spark chambers, carrying almost all the energy of the original e^+e^- pair, and these two electrons remain with very low energy.

We estimate that the ratio $r = \gamma/e$ among the real events $e^+e^- \rightarrow \gamma\gamma$ and these fake $e^+e^- \gamma\gamma$ events is always rather small. At $E = 400$ MeV, and $\theta = 90^\circ$, $r \cong 2 \times 10^4$. At angles of the order of $\theta = 20^\circ$, we obtain $r \cong 25$. This effect depends on the thickness of the donut and may become important at $\theta \lesssim 10^\circ$.

c) Another accidental coincidence could happen between a true $\gamma\gamma$ event and a single bremsstrahlung photon in the 0° counter (§5), coming from another electron positron or from an electron-gas interaction. This photon could of course be confused with our third photon. Assuming a total cross section at 0° of 5×10^{-25} cm^2 at $E = 1.5$ GeV, corresponding to a lower detection threshold $\simeq 0.01\,E$ in the energy spectrum of the radiated photon, one finds that the number of cases in which a $\gamma\gamma$ event in the chambers will be accompanied by a third photon in the 0° counter is $\simeq 6\,^o/_{oo}$ of the total true $\gamma\gamma$ number of events.

This percentage is a factor 10 or more lower than the true photon ($\gamma\gamma$ + radiative third photon) coincidences.

11. - TIME REQUEST. -

a) $e^+e^- \rightarrow \gamma\gamma$.

We continue to use here the formula $F(q^2) = (1 + q^2/Q^2)^{-1}$ to parametrize an eventual deviation from pure Q. E. D. Although not theoretically correct[4] this formula is useful to express the sensitivity of our apparatus to deviations from Q. E. D. In Table VI we report the percentage deviations of the counting rates calculated at various angles θ and for $E/Q = 0.1$ or 0.2. By percentage deviation we mean the percentage change in the cross section from $Q = \infty$ to Q equal respectively to 10 times and 5 times E.

The ratio between the percentage deviation and the percentage statistical error, when measuring for a time T at the energy E, goes like $(E^3/T)^{1/2}$ so that it is convenient to search for an eventual breakdown of Q. E. D. at the maximum energy of Adone. As one can see from table VI, if Q. E. D. holds, in 200 hours at 1500 MeV one can put an upper limit to Q of the order of $E/0,2 = 7.5$ GeV.

We will obtain the most probable value of Q from a χ^2 test

on the experimental angular distribution in θ. We will have as free parameters in the fit the absolute yield and the breakdown parameter Q, once the detection efficiency, the angular resolution and the radiative losses have been computed and included in theoretical (expected) rates (see also ref. (18)).

TABLE VI

θ (degrees)	Correction in % E/Q=0.1	E/Q=0.2	T = 200 hours and E = 1500 MeV Counts in the bin $\theta \pm 5^o$	Statistical error in %
20	-0.25	-1.0	330	±5.5
30	-0.57	-2.3	800	±3.5
40	-1.04	-4.2	700	±3.8
50	-1.66	-6.6	400	±5.0
60	-2.4	-9.6	---	---
70	-3.16	-12.6	130	±8.8
80	-3.76	-15.0	180	±7.4
90	-4.0	-16.0	160	±7.9
100	-3.76	-15.0	160	±7.9
110	-3.16	-12.6	200	±7.0
120	-2.4	-9.6	210	±6.9
130	-1.66	-6.6	---	---

This limit should go as $(E^3 T)^{1/4}$ so that, from the statistical point of view alone, it increases very slowly with the time of measure. However, because of systematic errors on radiative corrections, detection efficiency, angular resolution which enter in the measure and which are not yet estimated, these considerations are only of a semiquantitative nature.

Moreover, as a check of the apparatus, we think to take a first set of data at low energies where we should find the angular distribution predicted from pure Q. E. D. This could be done simultaneously to the investigation of the background for the $\pi^o \gamma$ and $\eta\gamma$ events, outside the ω and φ peaks (see next part).

The measurements at high energy shall be taken at least at 1000 and 1500 MeV, for a total machine time of 400 hours.

b) $e^+e^- \rightarrow \pi^o\gamma, \eta\gamma$.

b1) $\varphi \rightarrow \eta\gamma, \pi^o\gamma$ (E = 510 MeV, 11 eV/hour and 2 eV/hour respectively, at the maximum).

We plan to spend ~ 100 hours around the resonance. This should allow us to collect about 500-1000 $\eta\gamma$ events and so to achieve a precision on the cross section of the order of 5-10% when

errors on luminosity and experimental efficiency are included. In the mean time, according to the calculated rate, one should measure the $\varphi \to \pi^0\gamma$ cross section with a 10-20% accuracy.

For background measurement we will spend 60 hours taking measures outside the φ peak ($\pm$ 4 MeV).

b2) $\omega \to \eta\gamma$, $\pi^0\gamma$ (E = 390 MeV, 0.02 (?) and 8.8 events/hour respectively at the maximum).

We plan to spend $\sim$120 hours around the resonance. This corresponds to about 500-1000 $\pi^0\gamma$ events and consequently to a 5-10% accuracy of the cross section. For the $\omega \to \eta\gamma$ events, apart from background discrimination difficulties, one should give an upper limit for the cross section (of order of 10^{-32} cm^2).

For background measurement outside the ω peak we plan 80 hours.

b3) $\rho \to \eta\gamma$, $\pi^0\gamma$ (E = 382 $\pm$ 65 MeV, 0.017 and 0.08 events/hour respectively).

The expected ρ rates are very low, in any case they will be measured during the machine runs immediately outside the ω peak. A ρ-ω interference effect shall be present, however it seems that it should be hardly detectable[19]. Moreover about 60 hours will be devoted to measurements to the left and to the right of the ρ zone.

At higher energies, beyond the resonances, the time requested for reactions $e^+e^- \to \pi^0\gamma$, $\eta\gamma$ is included in the time necessary for observation of reaction $e^+e^- \to \gamma\gamma$. Therefore we plan at last 420 hours expressely dedicated for the study of reactions (2) and (3).

In conclusion our proposal requires a total of: 400 + 420 $\sim$ $\sim$ 800 hours with full luminosity of Adone. When one considers any possible uncertainty, including the beam lifetime, we consider convenient to ask for: 1000 hours.

The head of the Project office at the Physics Institute in Rome, ing. C. Cerlesi, has contributed to solve with original solutions our mechanics and optics problems and we are grateful to him and to his cooworkers Mr. Basti and Mr. Bronzini.

Our gratitude also to Mr. G. Di Stefano and his cooworkers of the High Energy workshop of the Frascati Laboratories, for their intelligent skill in the construction of the large dimensions spark chambers and counters of our apparatus.

REFERENCES AND FOOTNOTES. -

(1) - R. B. Blumenthal et al. Phys. Rev. Letters 14, 660 (1965).
(2) - J. C. Asbury et al. , Phys. Rev. Letters 18, 65 (1967); Phys. Rev. 161, 1344 (1967); see also: A. Silverman et al. , Phys. Rev. Letters 17, 767 (1966).
(3) - R. Gatto, Proc. Intern. Symp. on Electron and Photon Interactions at High Energies, Hamburg (1965), vol. I, pag. 106; N. Cabibbo and R. Gatto, Phys. Rev. 124, 1577 (1961); Phys. Rev. Letters 4, 313 (1960); Nuovo Cimento 20, 184 (1961).
(4) - N. M. Kroll, Nuovo Cimento 45, 65 (1966); We add that a possible breakdown could depend also from other parameters these q^2, for instance $q \cdot k$, k being the momentum of the annihilation photon.
(5) - Y. S. Tsai , Phys. Rev. 137, 730 (1965); The radiative corrections for the experiments with Adone have been studied in a general way by: E. Etim, G. Pancheri and B. Touschek, LNF-66/38 (1966).
(6) - This value come out at the Heidelberg Conference (Sept. 1967), as a sort of "world average".
(7) - S. L. Glashow, Phys. Rev. Letters 11, 48 (1963) and bibl. We follow here the presentation of Glashow.
(8) - M. Gell-Mann, Phys. Rev. 125, 1067 (1962); J. J. Sakurai, Phys. Rev. Letters 9, 472 (1962).
(9) - P. L. Connolly et al. , Phys. Rev. Letters 10, 371 (1963); P. Schlein et al. , Phys. Rev. Letters 10, 368 (1963).
(10) - G. Di Giugno et al. , Nuovo Cimento 44A, 1272 (1966) and quoted bibl.
(11) - J. S. Lindsey and G. A. Smith, Phys. Letters 20, 93 (1966).
(12) - M. Badier et al. , Phys. Letters 17, 337 (1965).
(13) - R. H. Dalitz, Summer course at Les Houches (1965). In the following we follow his calculations and bibliography; For the original work on the non relativistic quark model see : C. Becchi and G. Morpurgo, Phys. Rev. 140B, 687 (1965); G. Morpurgo, Phys. Letters 20, 684 (1966); 22 214 (1966); Acta Phys. Hungarica 22, 105 (1967).
(14) - This point was underlined to one of us by N. Cabibbo. We are grateful to N. Cabibbo for enlightening discussions on the $V \rightarrow \rightarrow P + \gamma$ decays.
(15) - Shui Yin Lo, Phys. Rev. 148, 1431 (1966).
(16) - V. V. Barmin et al. , Phys. Letters 24B, 249 (1967).
(17) - G. Altarelli and F. Buccella, Nuovo Cimento 34, 1337 (1964).
(18) - U. Amaldi et al. , Report ISS-66/1 (1966).
(19) - N. Cabibbo, private communication.

APPENDIX A - Experimental determination of the photon detection efficiency and of the angular resolving power of our apparatus.

As we already said, it is very important to know which are for our experimental apparatus the photon detection efficiency (in function of the energy and of the converter thickness) and the accuracy attainable in the measure of the photon direction.

For this aim we set up, behind the pair spectrometer of the synchrotron, a simple apparatus which allows to have monocromatic photons (see Fig. A. 1).

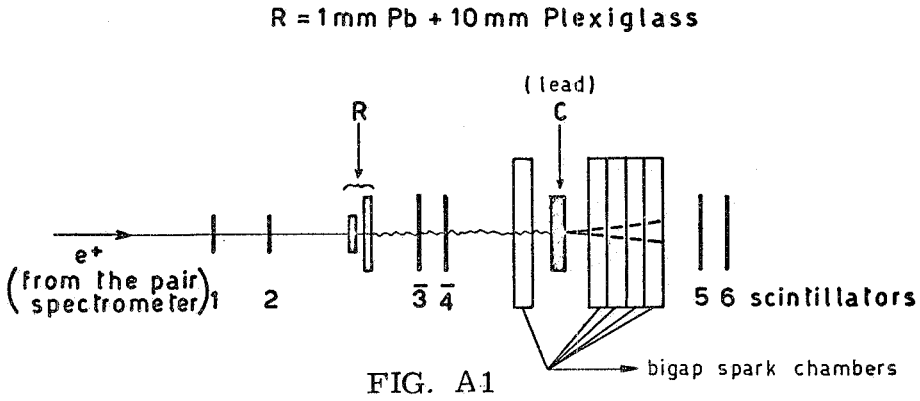

FIG. A1

Counters 1, 2 define an electron of known energy; a photon of the same energy emitted by this electron in the radiator R is defined by the coincidence $1+2+(\bar{3},\bar{4})$. The small thickness of the radiator (0. 2 R. L.) and the presence of the veto counters 3, 4 garantee us that practically all the energy of the initial electron is taken away by the bremsstrahlung photon (really in some case two hard photons are emitted).

In this maner we obtain photons of any desired energy from 50 MeV up to 900 MeV with an energy spread $\Delta K \simeq 5$ MeV.

These photons have the same direction of the electrons apart a very small angular spread due to the scattering in counters 1, 2 and in R and to the natural emission angle: all this accounts for an error $\Delta\theta \simeq 1^{o}$ at 500 MeV.

With this method we obtain ~ 0.004 photons per incident electron and this corresponds to ~ 1000 photons per minute at a 200 MeV energy. At higher energies we have lower counting rates.

1. - Measurement of the direction of the photons.

We have placed between counters 3, 4 and 5, 6 a set of spark chambers and converters and we have taken the pictures of the sho-

wers initiated in the converter C, triggering with the coincidence $1+2+(\overline{3}, \overline{4})+5+6$.

We took photos of the vertical view. In this view the electrons and photons must have all the same direction, because they lie in the median plane of the spectrometer, apart from small scattering effects.

We have films for various arrangements of the spark chambers and of the converters. We report here the results obtained for the disposition shown in Fig. A1. This disposition is essentially the one adopted in experimental apparatus of Fig. 8.

The pictures of the showers, when the thickness of C does not exceed 1 - 2 R. L., generally contain only few tracks of the first $e^+ e^-$ pairs.

In a first approximation we have taken the showers axis as giving the photon direction. In Fig. A2 is shown the distribution of the photon direction respect to the one of the initial electron: these data were taken at an energy of 500 MeV, with a thickness of C equal to 10 mm of Pb. We also took photos of the electron tracks (with the radiator R and without the converter C) and in Fig. A3 we give the corresponding distribution of the directions measured on the film.

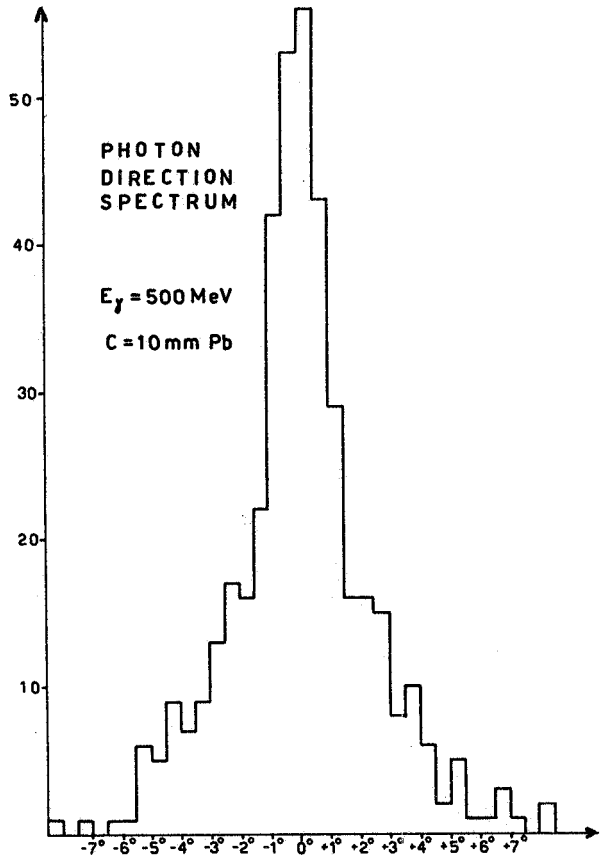

FIG. A2

The same pictures have also been scanned with the automatic scanning system of the Frascati Laboratories(x); as an example we report in Fig. A3b the results obtained for the electrons of 500 MeV. The Figures A3 and A3b refer to the same film. In the case of the automatic scanning we have a wider angular distribution because in the programs are not yet per-

(x) - F. Pandarese e M. Spinetti, LNF-67/25 (1967).

fectionated the criteria for rejecting spurious or misleading sparks.

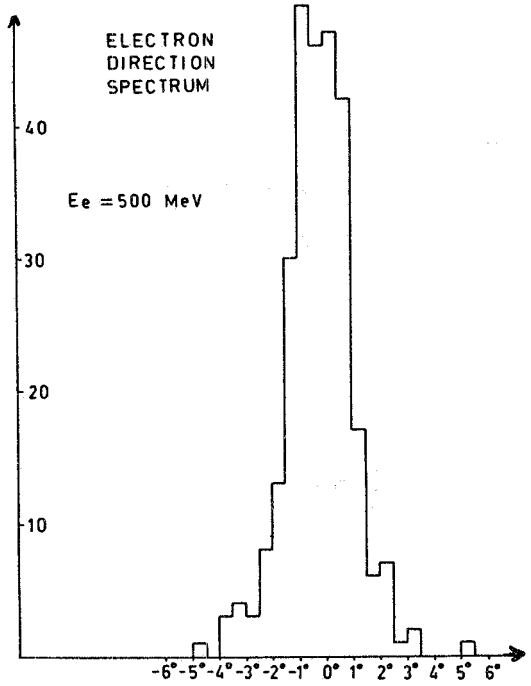

FIG. A3

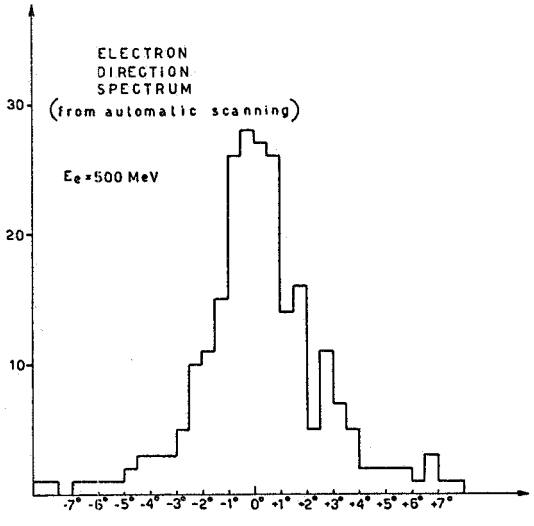

FIG. A3b

2. - Efficiency measurements.

Using the same apparatus, we measured the detection efficiency for various thicknesses of the converter C (lead). The spark chambers were simulated by a constant Aluminum absorber of 24 mm. The detection efficiency is defined by the ratio :

$$\frac{1 + 2 + (\bar{3}, \bar{4}) + 5 + 6}{1 + 2 + (\bar{3}, \bar{4})} = \frac{\text{showers}}{\text{photons}} \quad .$$

In Fig. A4 is shown(x) the detection efficiency versus the converter thickness at the energies 200, 500, 800 MeV.

If we put between counters 5 and 6 a lead layer of 10 mm the detection efficiency is left unchanged for photons of energy greater than $\sim$ 400 MeV while it decreases for photons of lower energy.

This effect together with the use of an eventual lead shielding to put around the donut could help us in reducing the sensibility of our apparatus to the background.

In Fig. A5 is given the detection efficiency for photons which have passed through 10-50-100 mm Pb before reaching the detection apparatus.

(x) - These results must be slightly corrected for the effect of simultaneous emission of two hard photons in R.

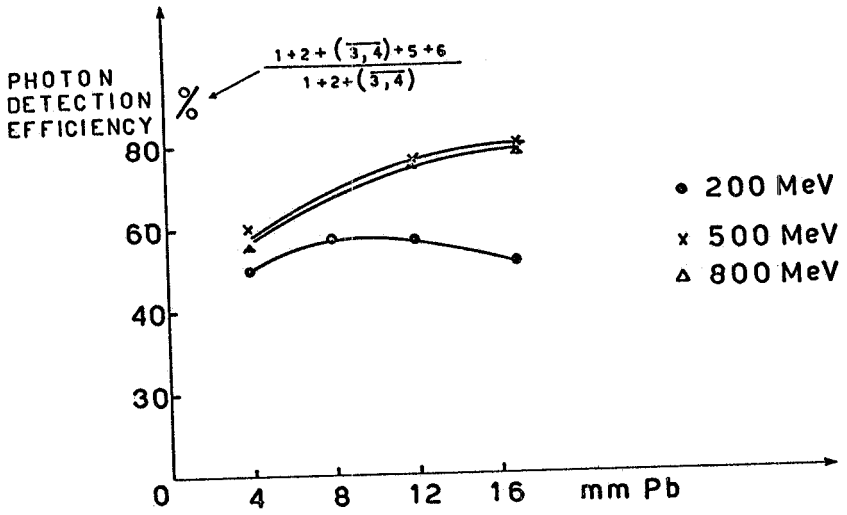
PHOTON
DETECTION
EFFICIENCY
%
1+2+(3,4)+5+6 / 1+2+(3,4)
80
60
40
30
0
4
8
12
16
mm Pb
• 200 MeV
x 500 MeV
△ 800 MeV

FIG. A4

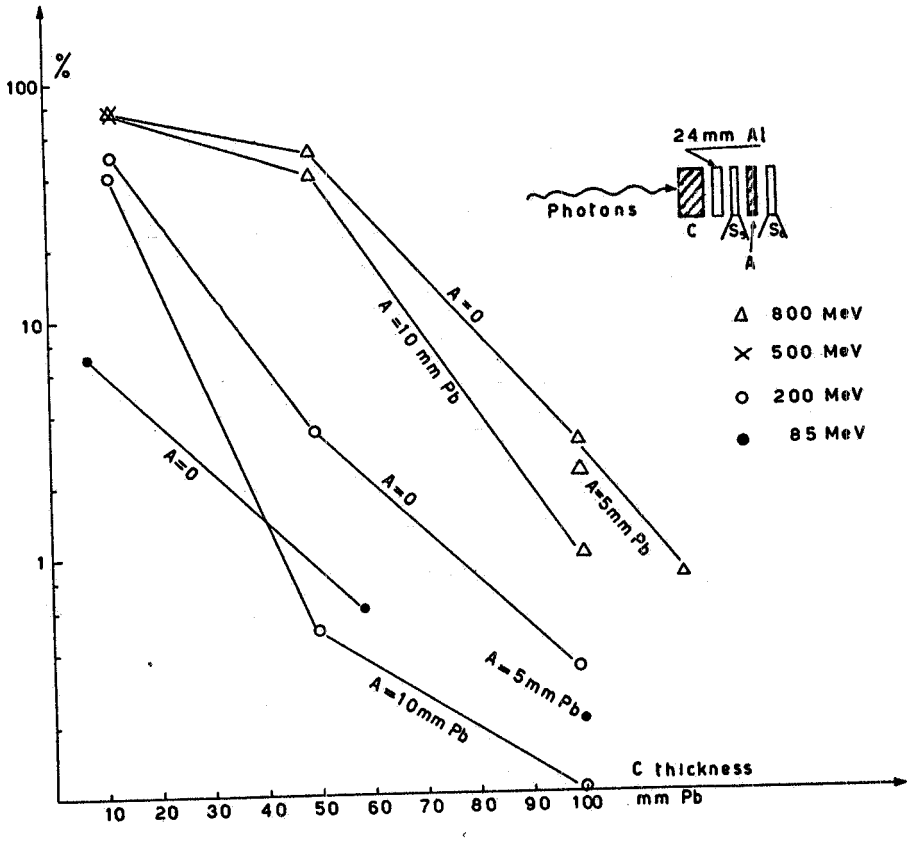
%
100
10
1
24mm Al
Photons
C
S1
S2
A
△ 800 MeV
× 500 MeV
○ 200 MeV
● 85 MeV
A=0
A=10 mm Pb
A=5mm Pb
A=0
A=0
A=5mm Pb
A=10mm Pb
C thickness
mm Pb
10 20 30 40 50 60 70 80 90 100

FIG. A5

These measures concern not only the problem of background rejection but also are important to establish how much lead will be necessary in a protection "roof" against cosmic rays to avoid that a "good" photon could trigger the anticoincidence counter (see Fig. 8).

All these measures are in progress and will be published in a next future.

APPENDIX B - Evaluation of the detection efficiency by a Montecarlo method.

For evaluating the cross section of the annihilation process $e^+ + e^- \rightarrow \gamma + \gamma$ from the experimental data, it is necessary to know the efficiency of detection of this process by the experimental apparatus. This efficiency is the product of the geometrical efficiency and the physical efficiency: the first one can be easily calculated, once the dimensions and the position of the counters are known. The second one is defined as the efficiency of detection of a photon by the given scintillation counter telescope. This physical efficiency depends on the material used as radiator between the scintillation counters, on its thickness, and on the logic of the electronics connecting the counters.

For evaluating this physical efficiency, we have simulated, with a 7040 computer using the Montecarlo method, the development of an electromagnetic shower initiated by a photon, in lead. We have supposed that the dimensions of the material, normally to the shower axis were infinite, so that no edge effect due to lateral losses was taken into account.

The development of the shower was followed up to a depth of 19 radiation length (R. L.) of lead. The processes taken into account are: bremsstrahlung, pair creation, Compton effect on the nucleus, Coulomb scattering and ionization losses.

The cross sections for these processes have been taken from B. Rossi(x) and E. Segrè(o). The angular distribution of the Coulomb scattering has been considered as gaussian.

The shower development was followed in two dimensions, that is in a plane containing the shower axis, by projecting each particle track of the shower on this plane. This simplifies the calculation, introducing a negligible error in the final result.

(x) - B. Rossi, High Energy Particles (Prentice Hall, 1952).
(o) - E. Segrè, Experimental Nuclear Physics (Wiley, 1953).

For the evaluation of the detection efficiency we supposed that the 19 R. L. radiator was divided into 39 slices each one separated from the other by a scintillation counter. The thickness of the slices was 0. 25 R. L. for the first 20 slices; 0. 5 R. L. for the next 10 slices; and 1 R. L. for the last 9 slices. In such a way we simulate a telescope of 40 counters: one between each slice, plus one in front of the radiator.

For a given incident photon energy (E_o), and at a given depth (t in R. L.) in the radiator we consider as dead all the electrons and photons with energy lower than E. The calculation was carried out for the following values of E_o and E.

E_o = 200 MeV ; E = 5, 10, 15, 20 MeV

E_o = 500 MeV ; E = 5, 10 MeV

E_o = 1000 MeV ; E = 5, 10 MeV

E_o = 1500 MeV ; E = 5, 10 MeV

By accumulating a statistics of 2000 events for each set of values of E_o and E, we obtain the following information :

1) Probability of having n electrons at a given depth t;
2) Average number ($\bar{n}$) of electrons as a function of the depth (t);
3) Probability ($\mathcal{E}_1$) of detection of a photon by one counter placed at a depth t in the radiator;
4) Probability ($\mathcal{E}_{12}$) of detection of a photon by two counters in coincidence placed at a depth t_1 and t_2 respectively;
5) Probability ($\mathcal{E}_{123}$) of detection of a photon by three counters in coincidence placed at a depth t_1, t_2, t_3 respectively.

t_1, t_2, t_3 are considered in the range from zero to 19 R. L.

We have checked our results by comparing the curve with the existing calculations(x). The agreement is sufficiently good (see Fig. B1).

Typical efficiency curves obtained for single and double coincidence are shown in Figg. B2 and B3 respectively. From Fig. B3 we can deduce the best arrangement for counters and radiators to obtain the maximum detection efficiency, for a telescope of two counters in coincidence. In fact we observe (Fig. B3) that for a given thickness of radiator ($\Delta t = t_2 - t_1$) between counter 1 and counter 2 there is an optimal value for the thickness of the radiator (t_1) in front of counter 1, corresponding to the maximum of the curves

---

(x) - D. F. Crawford and H. Messel, Phys. Rev. 128, 2352 (1962);
- H. H. Nagel, Z. Phys. 186, 319 (1965);
- U. Völkel, Report DESY 67/16 (1967).

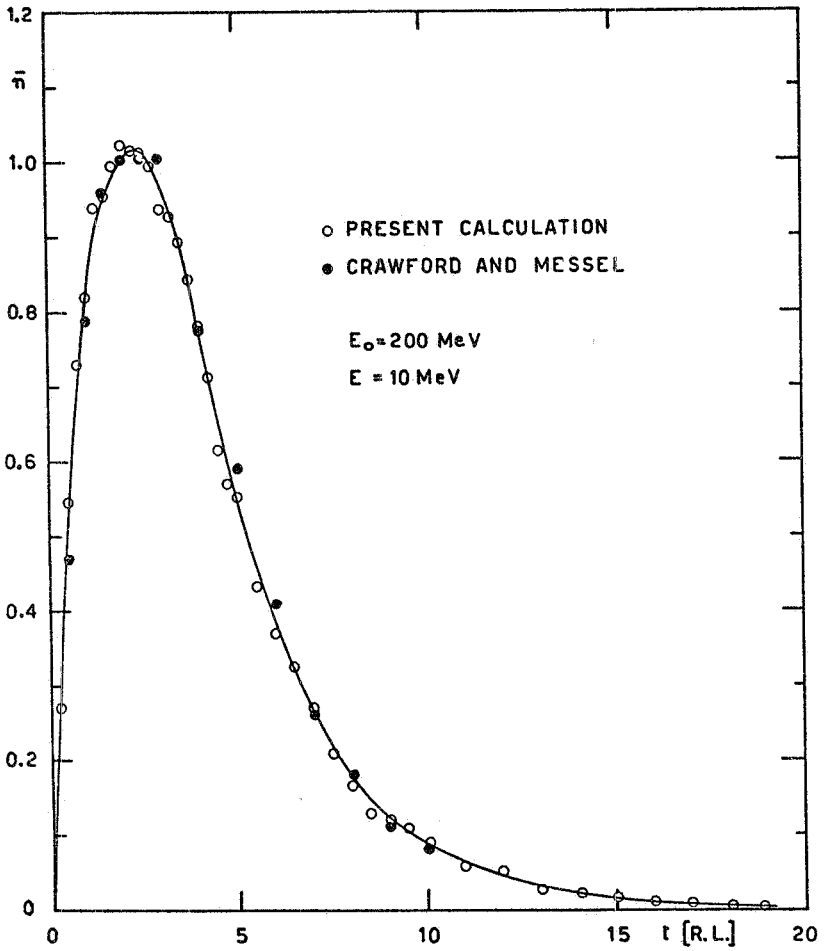
1.2
$\bar{n}$
1.0
0.8
0.6
0.4
0.2
0
0
5
10
15
t [R.L.]
20
○ PRESENT CALCULATION
● CRAWFORD AND MESSEL
E_o=200 MeV
E = 10 MeV

FIG. B1

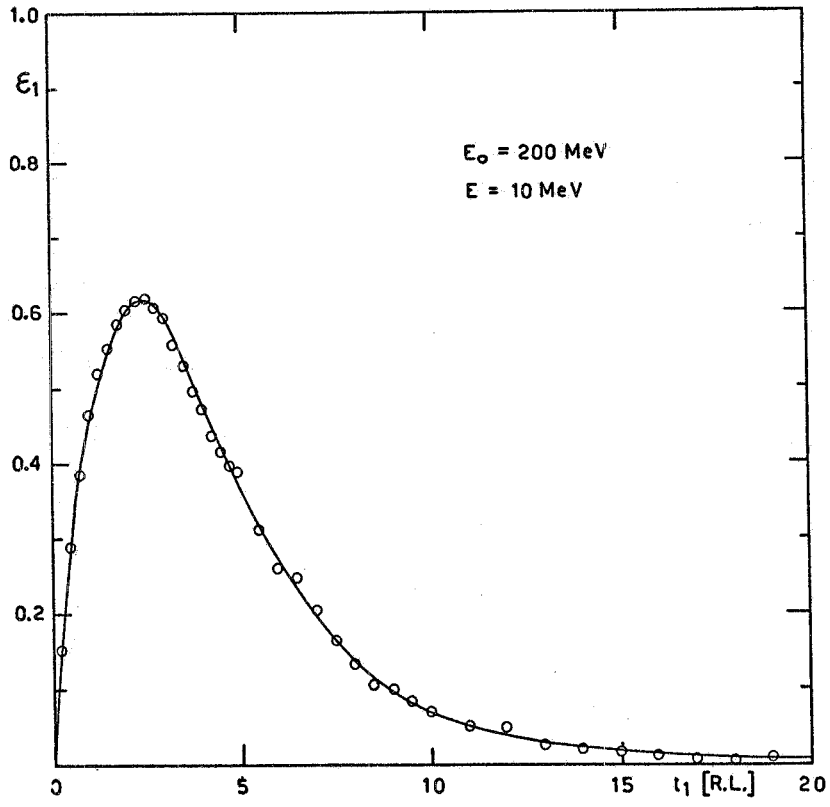
1.0
ε_1
0.8
0.6
0.4
0.2
0
5
10
15
t_1 [R.L.]
20
E_o = 200 MeV
E = 10 MeV

FIG. B2

of Fig. B3.

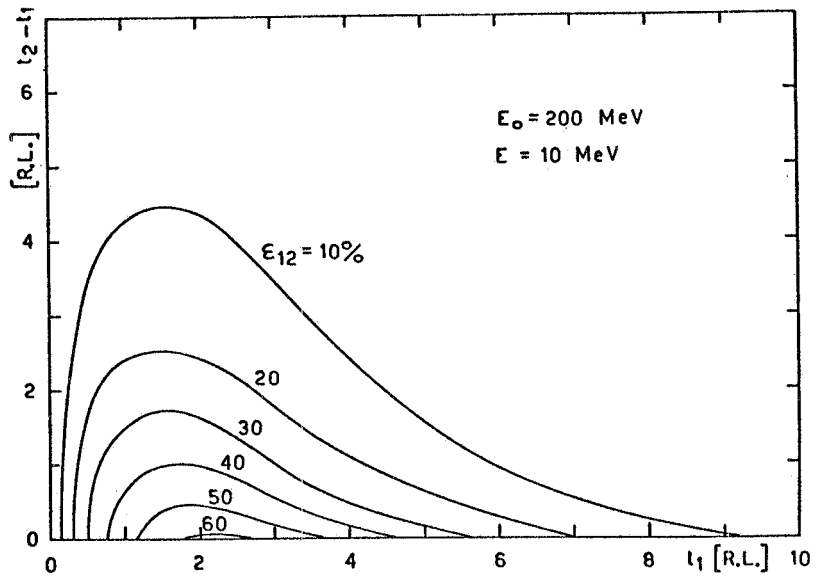

FIG. B3

Finally we report in Figg. B4 and B5 a tipical set of efficiency curves for a three-fold coincidence.

Experimental measurements are in progress at the Frascati synchrotron for checking, if possible, the Montecarlo calculation.

APPENDIX C - On cosmic rays rejection.

The geometrical disposition, essentially horizontal, of our detecting apparatus makes particularly important the problem of rejecting the cosmic ray triggers. In this respect a time-of-flight analysis system has been built such that a discrimination between "Adone type" events and cosmic rays crossing the apparatus is possible on the basis of the difference in time of flight. This method, already pointed out and studied for relatively small counters (30x x60 cm^2) by Paoluzi and Visentin(x), has been extended to large size scintillation counters (1.16 x 1.16 m^2) at a relative distance of about 2 m.

The basic idea is to cover the experimental apparatus with two horizontal large size counter systems a and b (see Fig. C1) placed above and underneath respectively.

(x) - Nota LNF-67/31 (1967).

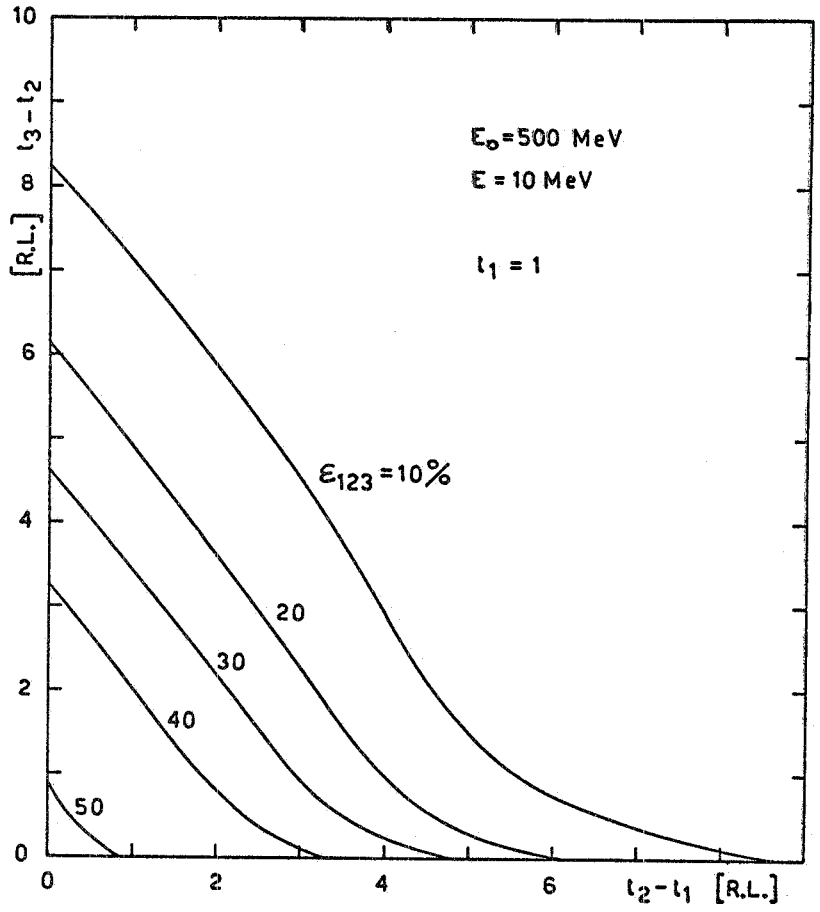
E_o=500 MeV
E = 10 MeV
t_1 = 1
ε_{123}=10%
20
30
40
50
t_3-t_2 [R.L.]
t_2-t_1 [R.L.]
0
2
4
6
8
10

FIG. B4

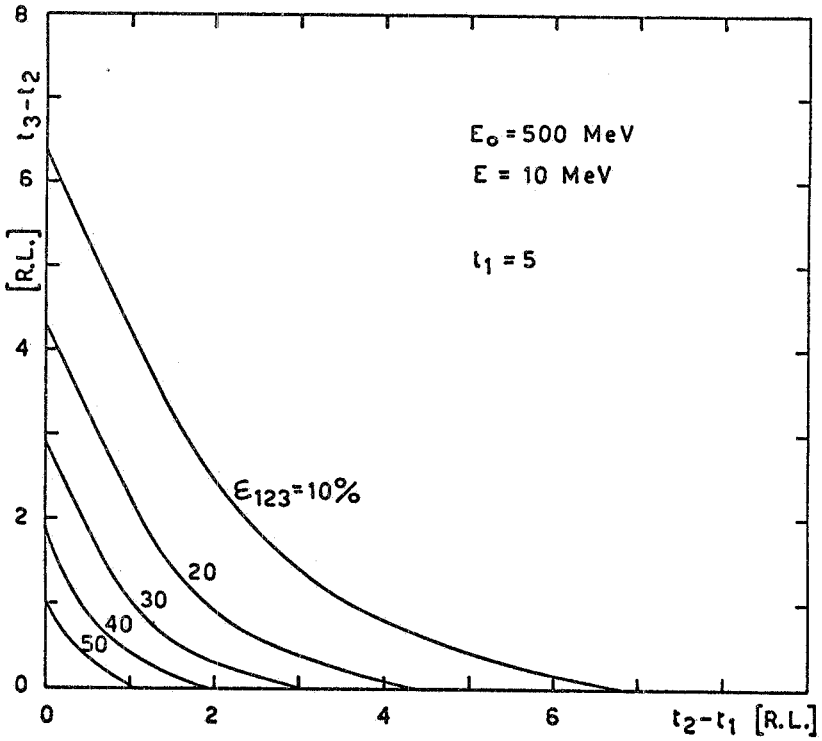
E_o=500 MeV
E = 10 MeV
t_1 = 5
ε_{123}=10%
20
30
40
50
t_3-t_2 [R.L.]
t_2-t_1 [R.L.]
0
2
4
6
8

FIG. B5

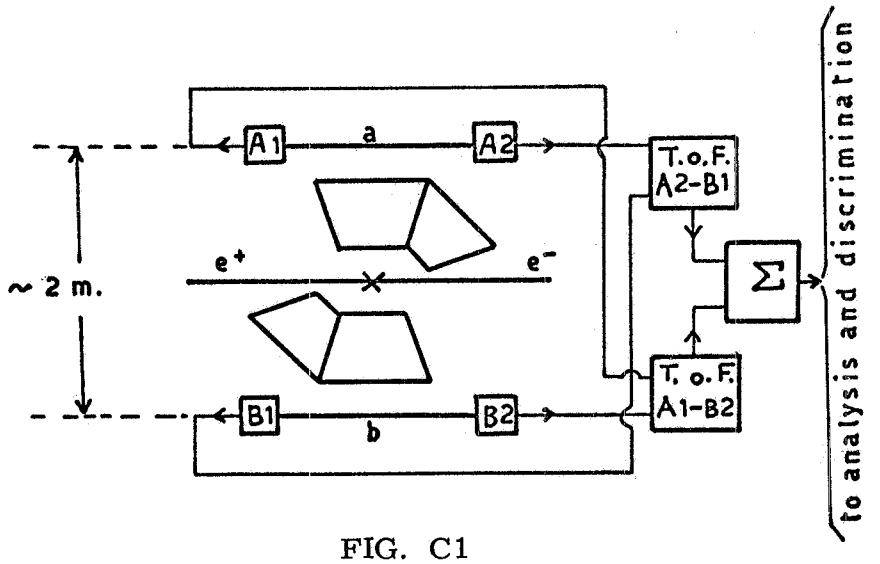

FIG. C1

Each of the scintillators a and b is viewed by two phototubes, one at each end (A1 and A2, B1 and B2 respectively). The large size of the scintillators would make the time-of-flight resolution quite poor. To compensate for this effect and to get the good time resolution requested, two times-of-flight are measured, one by using phototubes A1 and B2 and the other by using A2 and B1. These two times-of-flight are electronically added (box Σ in Fig. C1), then analyzed and used for the proper discrimination between "Adone type" events (average time difference around zero) and cosmic μ mesons (average time-of-flight of the order of 6-7 nsec).

A typical time-of-flight distribution as registered in a multichannel pulse height analyzer with a sensitivity of $\sim$ 20 channels/nsec is shown in Fig. C2.

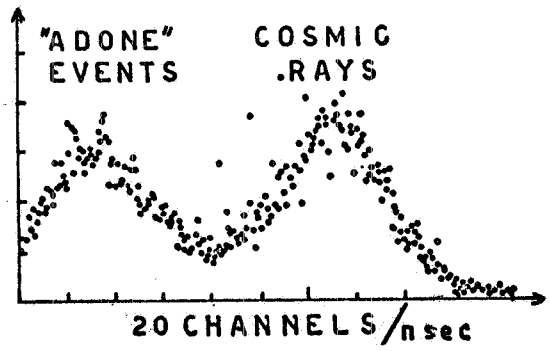

FIG. C2

The first peak simulates "Adone type" events and is obtained by putting the two counters a and b very close one to the other (time-of-flight practically zero); the second peak, labeled "cosmic," is due to cosmic μ mesons crossing the apparatus when the distance between the two counters is $\sim$ 2 m. The quasi-gaussian shape of the time-of-flight distributions with their typical total widths of $\sim$ 3 nsec allow us to believe that in our geometrical disposition a cosmic ray rejection of $\sim$ 80% with no loss of good events is possible.

APPENDIX D - Optics

Because of the large dimensions of our experimental apparatus respect to the available space in the experimental section of the ring, we have some trouble in the optics design especially as far as the dimensions and the support of the mirrors are concerned.

We considered two different arrangements for the mirrors: in the first one, the optical path, for both the chambers views, lies in the horizontal plane at the beams height (fig. D1, D2), while in the second one (which has been planned in case some obstacles are present) light is traveling at about 3 meters over the ring plane (fig. D3).

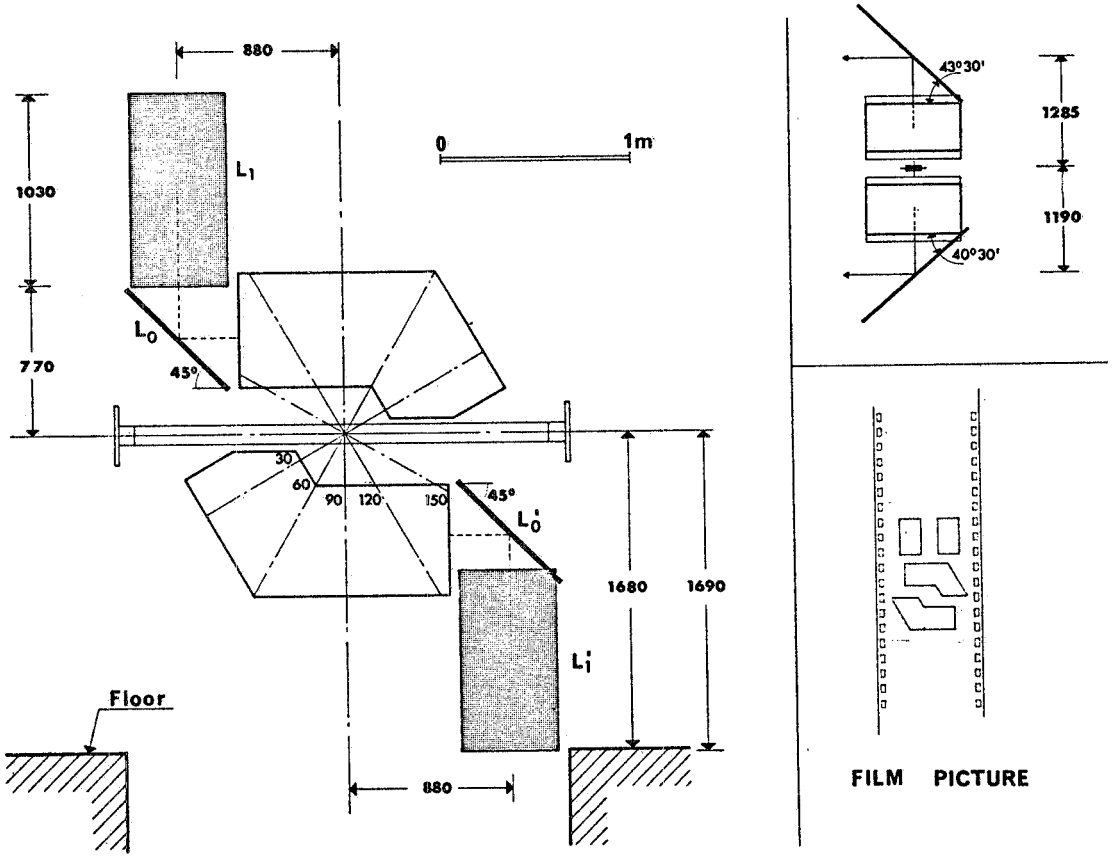

FIG. D1

As we said before the lateral view of the inclined chambers is obtained though a system of prisms (fig. D4). To reduce the distorsions and enlargements of the tracks in the lateral view, due to the overall thickness of the plexiglass at the junction between the horizontal and inclined chambers, it will be convenient to reduce the plexiglass frame of the chambers as much as possible.

We found in fact that the distorsion depends only from the plexiglass thickness and that any special optical flattening of the surfaces is of no aid.

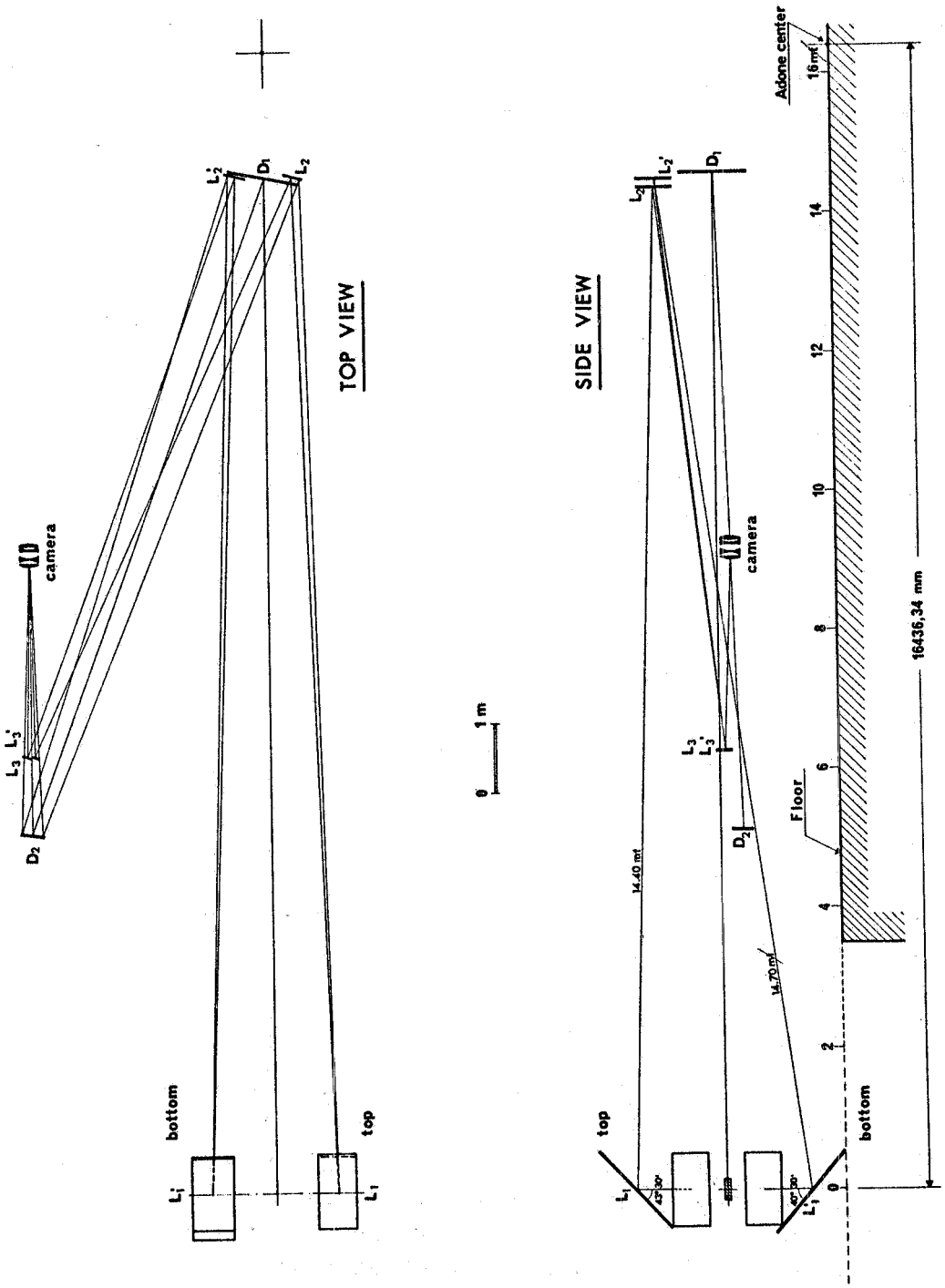
TOP VIEW
SIDE VIEW
camera
bottom
top
Floor
Adone center
16436,34 mm
14.40 mt
14.70 mt
0
1 m
2
4
6
8
10
12
14
16 mt

FIG. D2

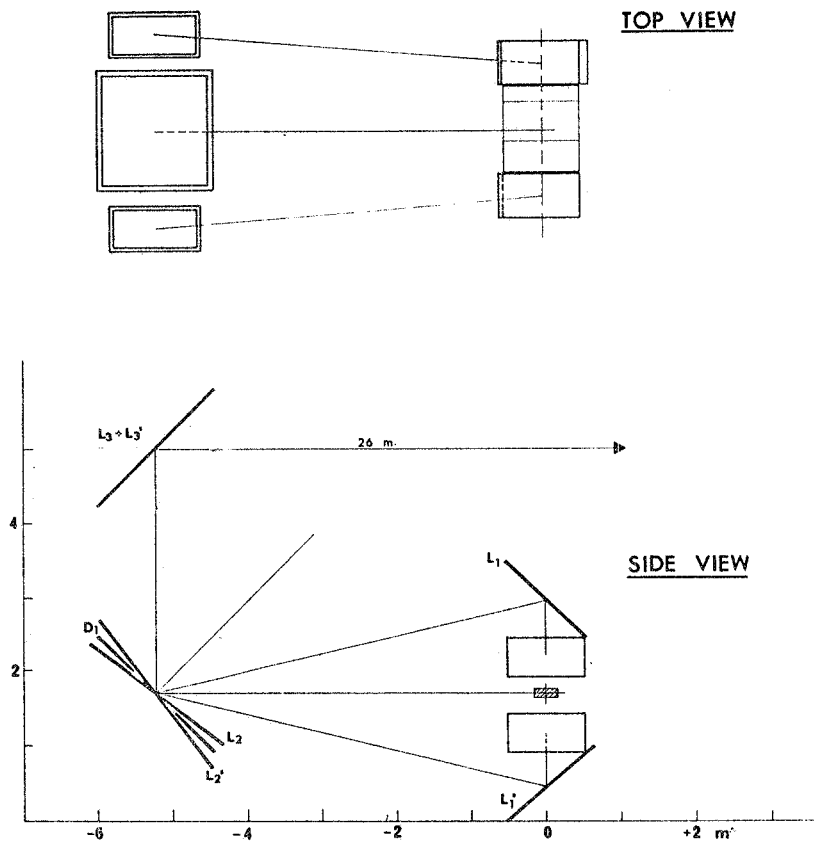
TOP VIEW
SIDE VIEW
L3 + L3'
26 m.
L1
D1
L2
L2'
L1'
4
2
-6
-4
-2
0
+2 m.

FIG. D3

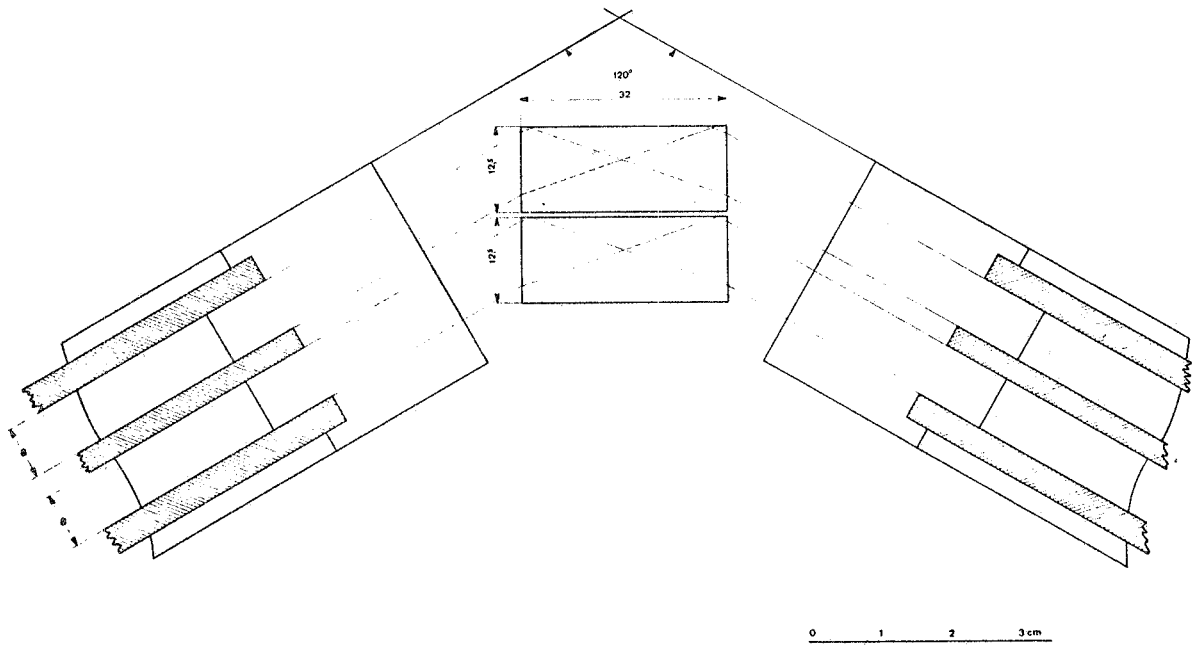
120°
32
12.5
12.5
0
1
2
3 cm

FIG. D4

The use of glass prisms instead of plexiglass ones should improve the situation: we will test this point.

A characteristics of our apparatus, from the optical point of view, is that cylindrical or spherical lenses will not be necessary in spite of the deepness of the chambers. In fact we plan to take pictures at great distance with an objective of large focal length, so as not to lose the more remote sparks in the chambers.

Preliminary tests made on this point are satisfactory: we took photos of cosmic rays tracks at a 26 m distance with a 600 mm focal length, and the sparks, for both the direct and the stereo view, are still quite visible on the film.

To have on the same film frame the direct and the stereo view of the chambers we shall use in the final optics a 900 mm objective and a 70 mm film. All the parts necessary for the 70 mm film are now being constructed and tested.

APPENDIX E - Comparison of the performance of different types of light pipe for a large area plastic scintillation counter.

The aim of these measures has been to compare the uniformity, the efficiency and the pulse height spectrum of a plastic scintillator NE 102 A of $90 \times 90 \times 2$ cm^3 when using different light pipes.

The scintillator was seen from only one side by two photomultipliers 56 AVP whose outputs where summed either passively or actively with a linear fan in. The voltage divider used was the standard one built for the Adone experiments.

We used four types of light pipes (see Fig. E1) :

1) a couple of traditional triangular plexiglass light pipes (tapered) of ~ 40 cm length;
2) a single flat rectangular plexiglass light pipe of dimensions $90 \times 45 \times 2$ cm^3;
3) a couple of flat square plexiglass light pipes each of dimensions $45 \times 45 \times 2$ cm^3;
4) a single light pipe in air, partially tapered, with reflecting internal cover of dimensions 90×45 cm^2.

We have studied the scintillator response for minimum ionizing cosmic rays defined by two plastic counters 15×15 cm^2 symmetrically placed respect to the scintillator plane at a relative distance of about 30-60 cm and which were jointly moved to explore different regions of the scintillator. The lower counter was shielded with 10 cm of lead (see Fig. E1).

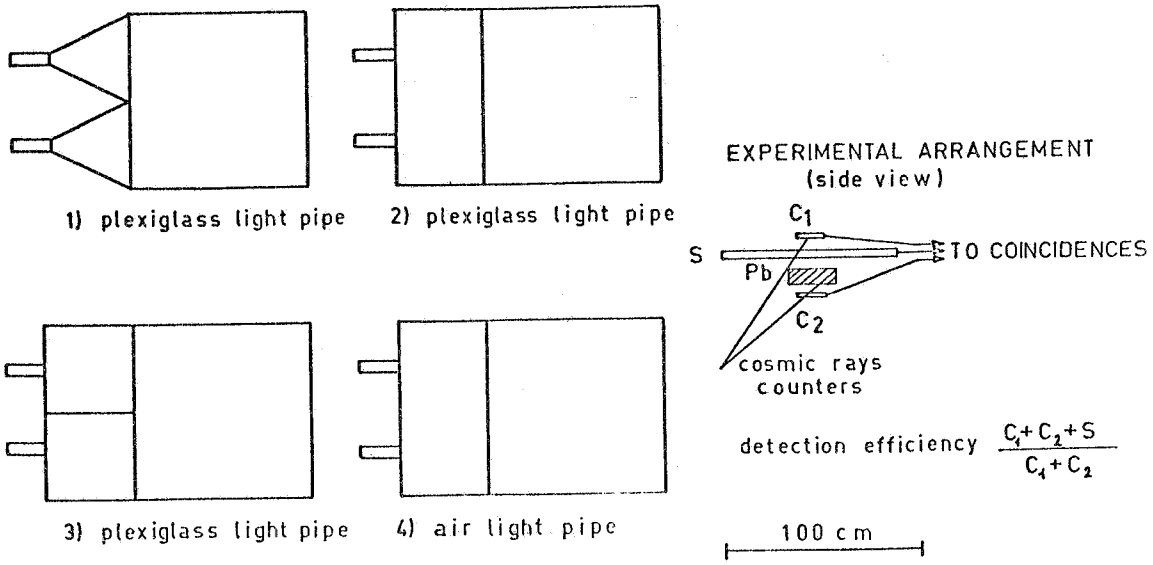

FIG. E1

We made the following measurements :

a) detection efficiency, taking the ratio between triple and double coincidence (see Fig. E1), in function of the position and of the H. V. ;
b) uniformity, measuring the current output when placing a gamma source (Co^{60}) on different points of the scintillator;
c) pulse height spectra. For this we checked that the photomultipliers pulse to light response was in the linear region and also the linearity of the electronics.

We found that the light pipes 1) and 2) worked the more satisfactorily and gave near equal results. In this case at 2500 V, with an electronic threshold of 0.4 V, and with the active sum of the two outputs we find an efficiency better than 99 % in any point of the scintillator. In these conditions we count also particles passing through the light pipes themselves with an efficiency of 30 % and 20 % for 1) and 2). The efficiency in function of the photomultiplier voltage is given in Fig. E2. In Fig. E2 are also shown the spectra taken at three different points of the scintillator.

Light pipe 3) was not as good as 1) and 2) while the air light pipe gave very poor results. In Fig. E3 are given the current measurement for all the four light pipes.

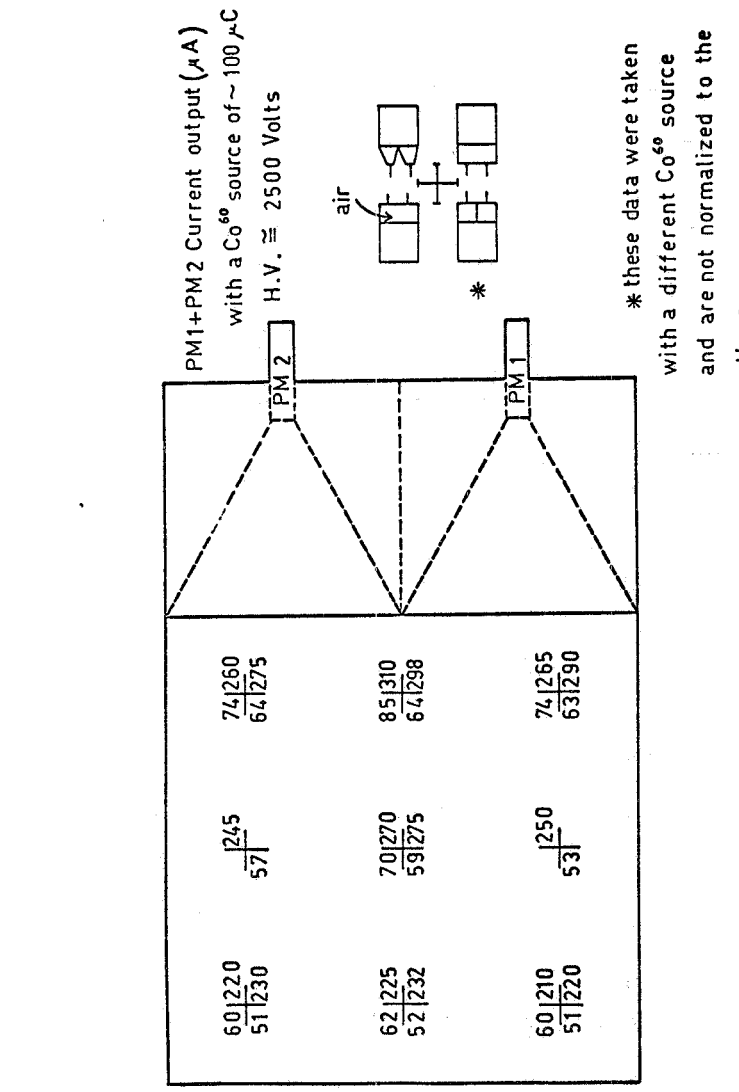
PM1+PM2 Current output (μA)
with a Co⁶⁰ source of ~ 100 μC
H.V. ≅ 2500 Volts
PM 2
PM 1
air
*
* these data were taken
with a different Co⁶⁰ source
and are not normalized to the
others.
60|220
51|230
|245
57|
74|260
64|275
62|225
52|232
70|270
59|275
85|310
64|298
60|210
51|220
|250
53|
74|265
63|290

FIG. E3

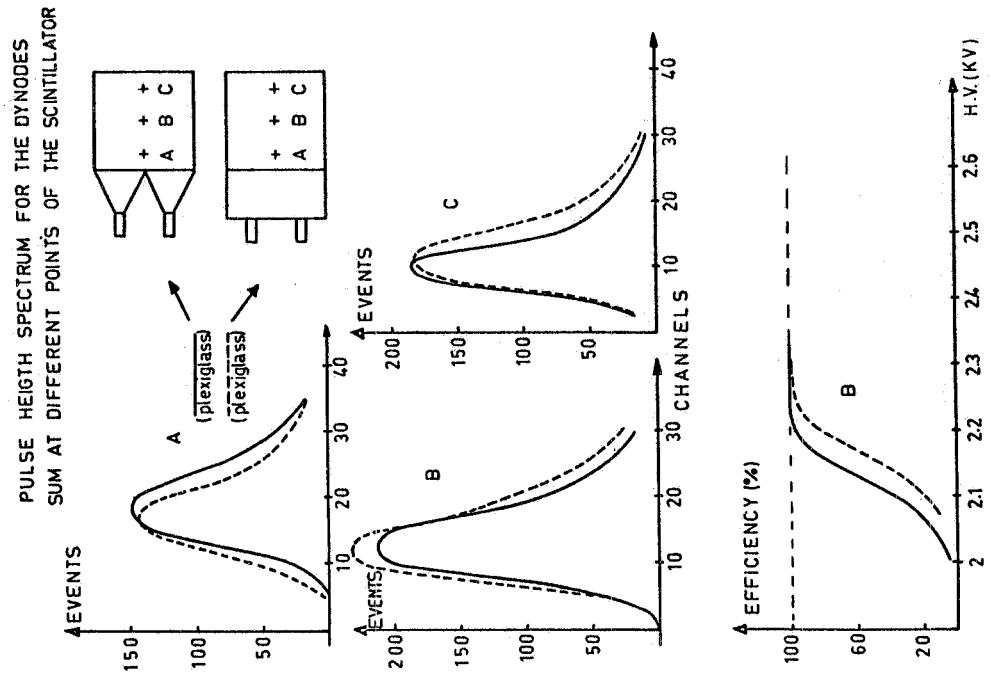
PULSE HEIGTH SPECTRUM FOR THE DYNODES
SUM AT DIFFERENT POINTS OF THE SCINTILLATOR
EVENTS
A
B
C
(plexiglass)
(plexiglass)
A B C
CHANNELS
EFFICIENCY (%)
H.V.(KV)

FIG. E2